

EUMETSAT Satellite Application Facility on
Support to Operational Hydrology and Water Management




Algorithm Theoretical Baseline Document (ATBD) for product SN-SWE-HH (H65)

Snow water equivalent by MW radiometry

Reference Number:	SAF/HSAF/ATBD-65
Issue/Revision Index:	1.2
Last Change:	11/11/2021


DOCUMENT CHANGE RECORD

Issue / Revision	Date	Description
1.0	4/1/2021	Baseline version prepared for PDCR
1.1	20/10/2021	Version revised according to PDCR
1.2	11/11/2021	Updated version (figure added) according to RID 034

	Algorithm Theoretical Baseline Document ATBD-65 (Product – SN-SWE-HH)	Doc.No: SAF/HSAF/ATBD-65 Rel. 1.2 Date: 11/11/2021 Page: 3/37
---	---	---

INDEX

1 Introduction to product SN-SWE-HH (H65)	4
1.1 Sensing principle	4
1.2 Main operational characteristics	5
1.3 Architecture of the products generation chain	6
1.4 Personnel	7
2 Processing concept	7
3 Algorithm description	9
3.5. Merging	26
4 Validation <i><if applicable></i>	27
5 Examples <i><if available></i>	27
6 Connections to other projects and future evolution of SWE products	27
EUMETSAT H SAF vs COPERNICUS	29
EUMETSAT H SAF vs ESA Snow CCI	29
7 References	30
Annex1: Introduction to H-SAF	33
The EUMETSAT Satellite Application Facilities	33
Purpose of the H-SAF	34
Products / Deliveries of the H-SAF	35
System Overview	35
Annex 2: Acronyms	36

	Algorithm Theoretical Baseline Document ATBD-65 (Product – SN-SWE-HH)	Doc.No: SAF/HSAF/ATBD-65 Rel. 1.2 Date: 11/11/2021 Page: 4/37
---	---	---

1 Introduction to product SN-SWE-HH (H65)

1.1 Sensing principle

Product SN-SWE-HH (H65) (Snow water equivalent by MW radiometry) is based on the SSMIS instrument onboard the DMSP series satellites. Conical scanners provide images with constant zenith angle, that implies constant optical path in the atmosphere and homogeneous impact of the polarisation effects. In addition, the SN-SWE-HH product is ready to utilize MWI instrument data on board MetOp-SG B once the satellite is launched.

Also, conical scanning provides constant resolution across the image, though changing with frequency. It is noted that the IFOV is elliptical, with major axis elongated along the viewing direction and the minor axis along-scan, approximately 2/3 of the major. As for the 'pixel', i.e. the area subtended as a consequence of the bi-dimensional sampling rate, the sampling distance along the satellite motion, i.e. from scan line to scan line, is invariably 10 km, dictated by the satellite velocity on the ground and the scan rate. Along scan, the sampling rate is 10 km for all channels except 89 GHz where is 5 km.

The SN-SWE-HH product is the result of an assimilation process for the non-mountainous areas. Data assimilated are 19V, 37V brightness temperature and station snow depth and density. The ground network of synoptic stations observing snow depth provides a first guess field that is converted into MW brightness temperatures by an emission model that also accounts for forests. The assimilation process forces the first guess field to optimally match the SSMIS brightness temperatures.

The retrieval algorithm is somewhat different for mountainous regions. Snow observations from ground network of synoptic stations are not used, snow density look up table is used when an unrealistic snow density is retrieved from the assimilation process. Data assimilated are 19V and 37V brightness temperature. SN-SWE-HH for flat and forested areas is generated in Finland by FMI and for mountainous areas in Turkey by TSMS. The products from FMI and TSMS both cover the Northern Hemisphere, but thereafter are merged at FMI by blending the information on flat/forested areas from the FMI product and that one on mountainous areas from the TSMS product, according to the mask shown in Figure 1.

For more information, please refer to the Products User Manual (specifically, volume PUM-65).

H65 Mountain Mask

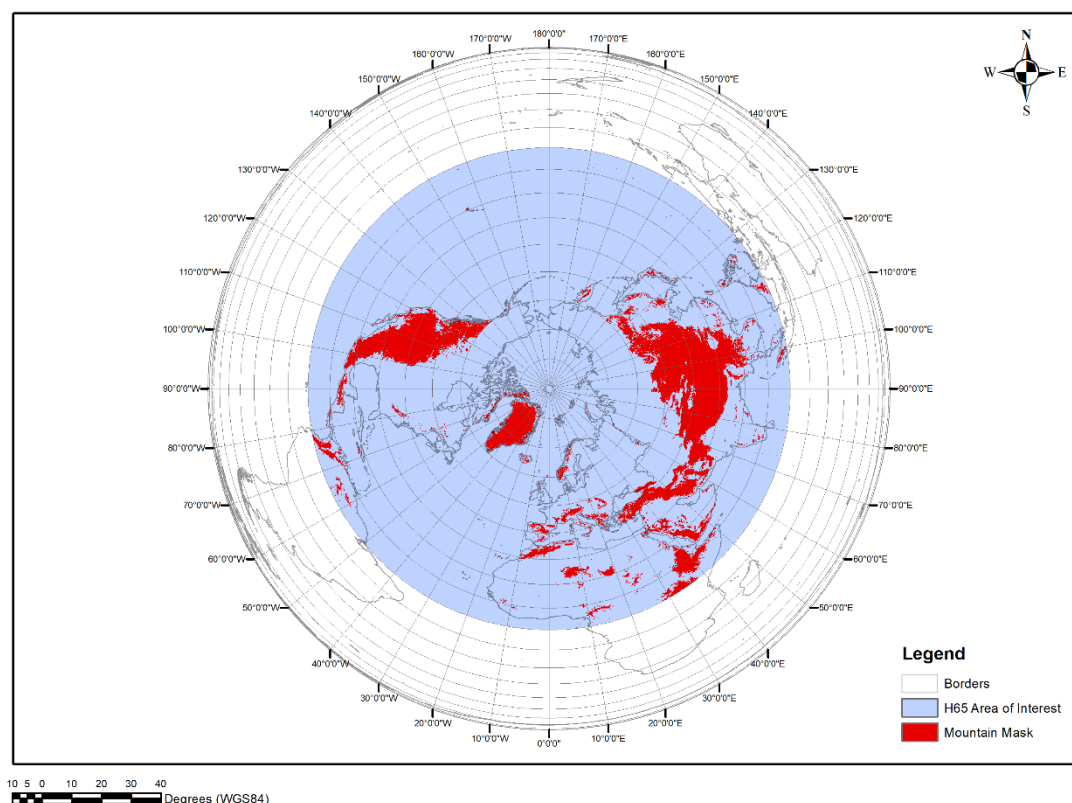


Figure 1 Mountain mask produced for H65 product

1.2 Main operational characteristics

The operational characteristics of SN-SWE-HH are discussed in PUM-65. Here are the main highlights.


The horizontal resolution (Δx). For MW conical scanners the IFOV is constant but depends on the frequency channels utilised for building the product. The current algorithm utilises the two frequencies 19.35 and 37.0 GHz, thus the resolution is that one of SSMIS at 19.35 GHz, i.e., ~ 20 km. Sampling is made at 0.25° intervals. Conclusion:

- resolution: $\Delta x \sim 20$ km - sampling distance: ~ 20 km.

The observing cycle (Δt). SSMIS is available on multiple satellites but only one is used. The swath is 1450 km, thus one satellite provides global coverage every 24 h. Conclusion:

- observing cycle: $\Delta t = 24$ h.

The timeliness (δ). For a product resulting from multi-temporal analysis disseminated at a fixed time of the day, the time of observation may change pixel by pixel (some pixel may have been cloud-free early in the time window, e.g. in the early morning, thus up to 12-h old at the time of dissemination;

	Algorithm Theoretical Baseline Document ATBD-65 (Product – SN-SWE-HH)	Doc.No: SAF/HSAF/ATBD-65 Rel. 1.2 Date: 11/11/2021 Page: 6/37
---	---	---

some very recently, just before product dissemination in the late afternoon). (<https://nwp-saf.eumetsat.int/site/monitoring/nrt-availability/data-timeliness/>) Thus the average timeliness is:

- -timeliness $\delta \sim 6$ h.

The accuracy is evaluated a-posteriori by means of the validation activity. See Product Validation Report PVR-65. For the MetOp-SG B MWI instrument the parameters are slightly different. The channels that will be used are MWI-1 (18.7 GHz) and MWI-3 (31.4 GHz). The SN-SWE-HH algorithm is scalable in terms of frequency and since the algorithm is also adaptive (assimilation) the slight frequency difference can be compensated. For the MWI-1 channel the footprint size of MWI is 50 km and for MWI-3 30 km. Since the lower frequency component is mainly for background level and the signal comes from MWI-3 (Chang et al. 1987) the nominal grid resolution of 25 km is achievable. The swath width of MWI is 1700 km that is somewhat more than in case of SSMIS.

The synoptic snow depth data are obtained operationally through FMI Near Real Time observation database and converted from object data format to CSV. The data is mainly derived from automated observations around the globe.

1.3 Architecture of the products generation chain

The architecture of the SN-SWE-HH product generation chain is shown in Figure 2.

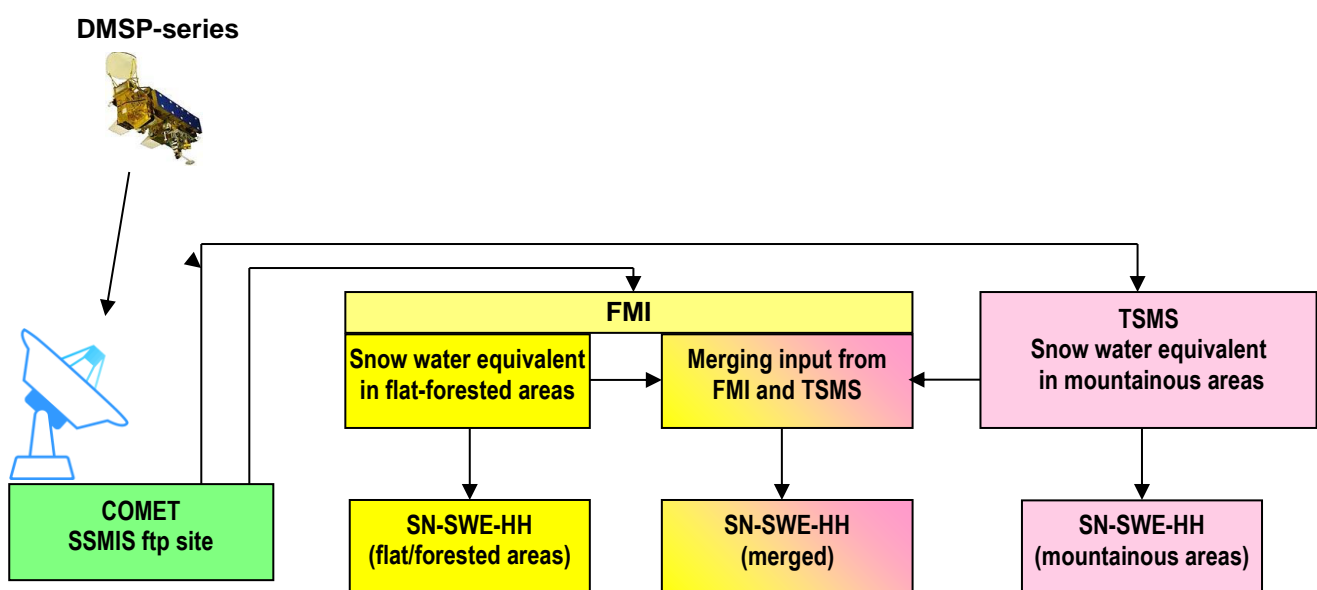


Figure 2 Conceptual architecture of the SN-SWE-HH chain.

The satellite data are acquired from the COMET or from EUMETCAST as an alternative. The product is generated both at FMI and at TSMS. The FMI product is tuned to flat/forested areas, that one from TSMS is tuned to mountainous areas. The TSMS data are delivered to FMI, that implements the merging of the two products according to the mask shown in Figure 1.

Currently, the products are held on the TSMS server (mountainous areas) and on the FMI and CNMCA servers (both flat/forested areas and merged). Eventually, only the merged product will be disseminated through EUMETCast.

1.4 Personnel

Names and coordinates of the main actors for SN-SWE-HH algorithm development and integration are listed in Table 1.

Table 1 Development team for product SN-SWE-HH

Jouni Pulliainen (Leader)	Finnish Meteorological Institute (FMI)	Finland	jouni.pulliainen@fmi.fi
Matias Takala			matias.takala@fmi.fi
Kari Luojus			kari.luojus@fmi.fi
Ali Nadir Arslan			ali.nadir.arslan@fmi.fi
Zuhal Akyürek	Middle East Technical University (METU)	Turkey	zakyurek@metu.edu.tr
Kenan Bolat	Turkish State Meteorological Service (TSMS)		kenan23@gmail.com
Sema Çil			semacil@mgm.gov.tr

2 Processing concept

The processing concepts for product SN-SWE-HH applied in Finland (FMI) and Turkey (METU) are very similar. HUT model as snow emission model is used in both algorithms. The main difference between the flat/forest and the mountain algorithms is the use of ground observations of snow depth (SD) at Synoptic observation stations for flat/forest algorithm. Both products are recorded independently.

2.1 Flat and forested areas

Figure 3 shows the flow diagram of the assimilation method for flat areas. First, 1) the SSMIS data is selected for the Synoptic observation station locations. 2) SSMIS data together with SD observations are used in the HUT model inversion to obtain an estimate of snow grain size (fitting parameter) for the station locations. 3) The snow grain size estimate (and error) are interpolated for the target area.

Next, 4) the SD observations are kriging interpolated for the target area. This gives the interpolated SD field and kriging error estimate.

In the next step 5) the snow grain size and error field, SD field and kriging error and SSMIS brightness temperature field together with auxiliary data such as snow climatology are used as input to the data assimilation step.

The result of the assimilation step 6) is the estimate of the SWE and the error of SWE retrieval. It is possible to use the SWE estimate from the previous day as an input in the assimilation step but this has been omitted (remains an option) in the operational implementation.

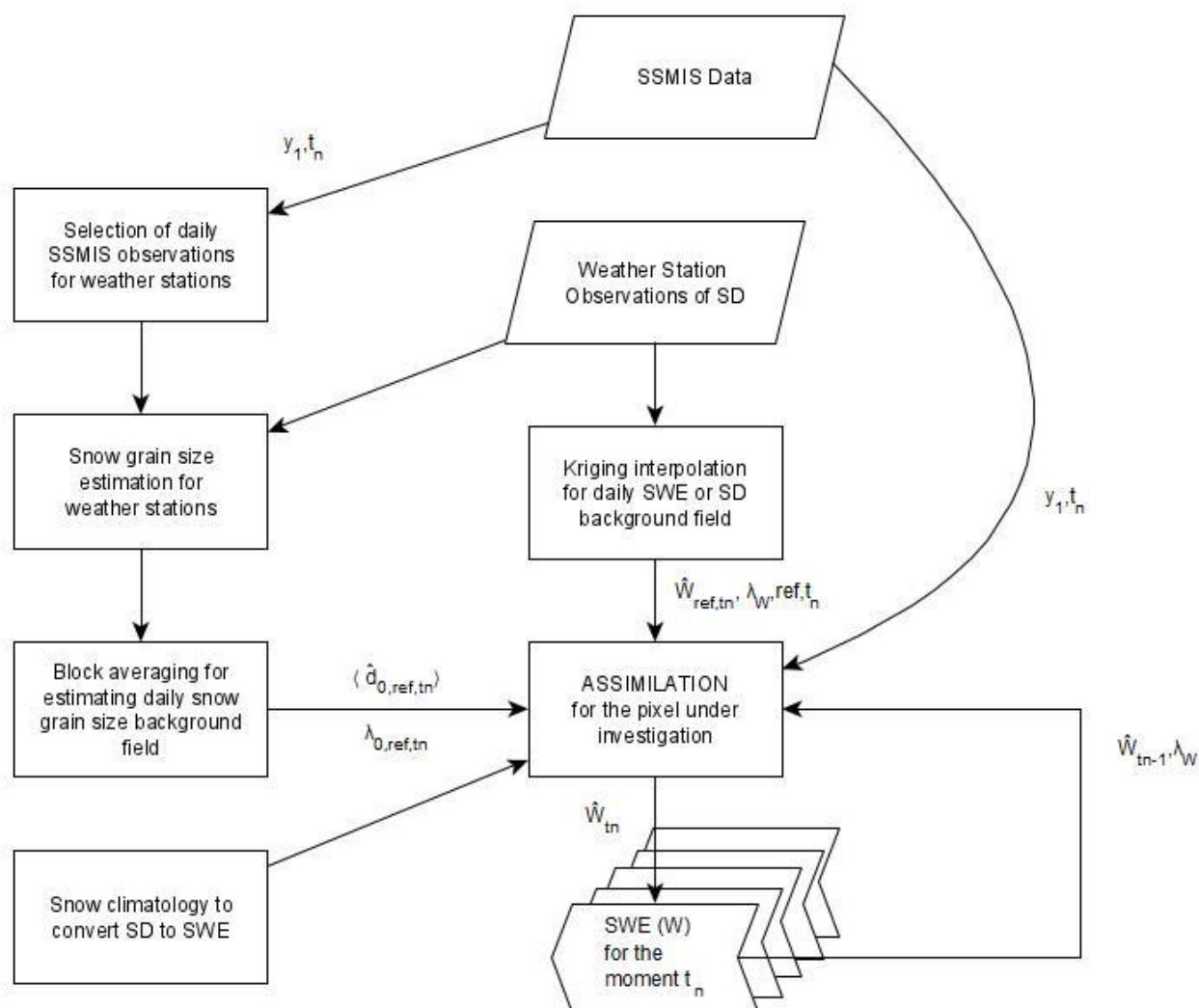


Figure 3 Flow diagram of the assimilation method in the case of SSMIS observations in flat/forested areas.

2.2 Mountainous regions

Figure 4 shows the flow diagram of the assimilation method, limited to the case of SSMIS observations that are currently used for snow water equivalent retrieval in mountainous regions.

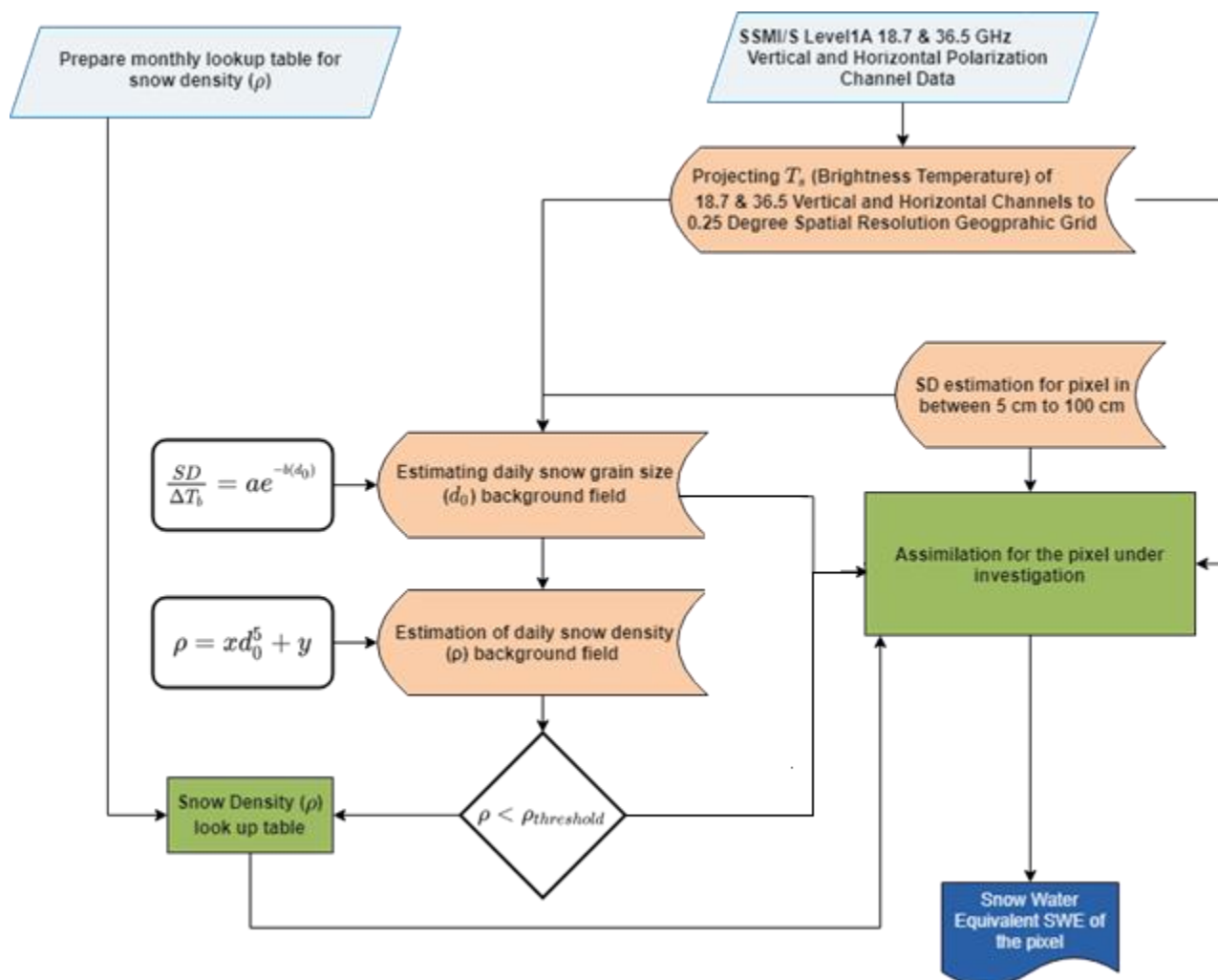


Figure 4 - Flow diagram of the assimilation method in the case of SSMIS observations in mountainous areas.

3 Algorithm description

3.1 Flat and forested areas

The HUT snow emission model

The HUT snow emission model describes the space-borne observed microwave brightness temperature as a function of snowpack characteristics and by considering the effects of atmosphere, forest canopy and land cover category (fractions of open and forested areas). A detailed description of the model and its performance is given by Pulliainen et al. 1999. The emission from a snowpack is modelled by applying the Delta-Eddington-approximation to the radiative transfer equation (considering the magnitude of forward scatter by an empirical coefficient). The snow layer is treated as single layer. The multiple reflections from snow-ground and snow-air boundaries are included using a non-coherent approach and the effect of forest canopy (transmissivity and emission) is included by employing an empirical model (Kruopis et al. 1999). Finally, the transmissivity and emission contributions of the atmosphere are included using a statistical atmospheric model (Pulliainen et al. 1993).

The input parameters of the HUT model include the snowpack characteristics (depth, density, effective grain size and temperature), soil properties (temperature, dielectric constant and effective rms height variation), forest canopy characteristics (stem volume/biomass) and near-surface air temperature dependent atmospheric emission and transmissivity contributions. The model formulation and its inversion are described in detail in (Takala et al. 2011). Table 2 summarizes typical values of adjustable model parameters as the HUT model is applied to the inversion of space-borne data. A summary of the inversion technique follows here. In addition, the input parameters for the HUT model used in the case of flat and forested areas are presented in Fig. 5.

Table 2 Pre-fixed HUT snow emission model parameter values for Northern Eurasia

Parameter	Value
Mean effective snow grain size, $\langle d_0 \rangle$ (mm)	1.3
Variance of d_0 , $\text{var}(d_0)$ (mm ²)	1.0
Variance of modeling error, $\text{var}(\epsilon_i)$ (K ²)	25
Variance of day-to-day SWE variation, $\text{var}(W)$ (mm ²)	25
Snowpack density (g/cm ³)	0.24
Effective soil surface roughness (mm)	3
Temperature, soil/snow/vegetation/near surface air (C °)	-5
Soil dielectric constant	6-1j

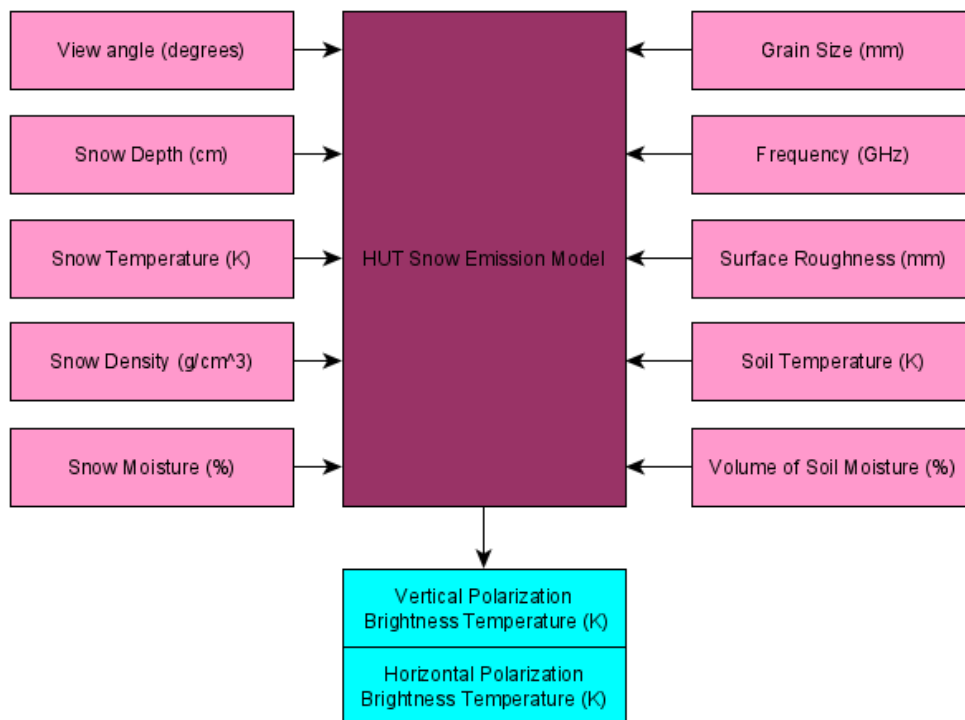



Figure 5 – The input parameters for the HUT model used in flat and forested areas

	Algorithm Theoretical Baseline Document ATBD-65 (Product – SN-SWE-HH)	Doc.No: SAF/HSAF/ATBD-65 Rel. 1.2 Date: 11/11/2021 Page: 11/ 37
---	---	--

Inversion of the snow emission model

Let the y_1 be the space-borne observed spectral and polarization brightness temperature difference:

$$y_1 = T_{b,19V,obs} - T_{b,37V,obs}, \quad (1)$$

where $T_{b,19V,obs}$ is the brightness temperature observed at a vertically polarized channel (close to) the frequency of 19 GHz and the second term is for 37 GHz.

The main snowpack characteristics affecting brightness temperatures at 19 and 37 GHz frequencies include the snow water equivalent, SWE, denoted here by W and the snow grain size (d_0). Brightness temperature differences according to (1) can be modelled by applying the HUT snow emission model. For simplicity we denote this direct modelling of channel differences by $f(\mathbf{x})$, where

$$\mathbf{x} = [W \quad d_0]^T \quad (2)$$

and thus

$$y = f(\mathbf{x}) + \varepsilon = \begin{bmatrix} f_1(\mathbf{x}) \\ f_2(\mathbf{x}) \end{bmatrix} + \begin{bmatrix} \varepsilon_1 \\ \varepsilon_2 \end{bmatrix}, \quad (3)$$

where ε is the vector of modelling error including the effect of instrument noise and all inaccuracies of modelling. If modelling error is assumed to be non-biased and normally distributed, the conditional probability density of satellite observations \mathbf{y} as a function of \mathbf{x} obeys the multidimensional normal distribution, refer to e.g. (Pulliainen and Hallikainen 2001; Pulliainen et al. 2004). Further on, as the Bayes' theorem is applied, we can write the expression for the conditional density of snow characteristics \mathbf{x} taking also into account possible *a priori* information on snow grain size (diameter):


$$\begin{aligned} \rho(\mathbf{x} | \mathbf{y}) &= \rho(W, d_0 | \mathbf{y}) \\ &\propto \exp \left\{ -\frac{1}{2} [\mathbf{y} - f(W, d_0)]^T \mathbf{C}^{-1} [\mathbf{y} - f(W, d_0)] - \frac{1}{2\text{var}(d_{0,\text{ref}})} (\hat{d}_{0,\text{ref}} - d_0)^2 \right\}, \end{aligned} \quad (4)$$

where *a priori* information suggests that d_0 is a normally distributed random variable with the expected value $\hat{d}_{0,\text{ref}}$ and variance $\text{var}(d_{0,\text{ref}})$. \mathbf{C} is the covariance matrix of modeling errors.

The maximum likelihood modeled estimate on W and d_0 is obtained by searching the global minimum of the absolute value of the exponent term given in (4), i.e. the minimum of the cost function $J(W, d_0)$:

$$J(W, d_0) = \left\{ \frac{1}{2} [\mathbf{y} - f(W, d_0)]^T \mathbf{C}^{-1} [\mathbf{y} - f(W, d_0)] + \frac{1}{2\text{var}(d_{0,\text{ref}})} (\hat{d}_{0,\text{ref}} - d_0)^2 \right\}. \quad (5)$$

Thus, the maximum likelihood estimate on SWE and grain size, $\hat{\mathbf{x}} = [\hat{W} \quad \hat{d}_0]^T$, must satisfy

	Algorithm Theoretical Baseline Document ATBD-65 (Product – SN-SWE-HH)	Doc.No: SAF/HSAF/ATBD-65 Rel. 1.2 Date: 11/11/2021 Page: 12/ 37
---	---	--

$$\left\{ \frac{\partial J(W=\hat{W}, d_0=\hat{d}_0)}{\partial d_0} = 0 \right\}. \quad (6)$$

As the HUT snow emission model is non-linear, the global minimum of (5) must be searched iteratively. If the correlation between modelling errors ε_1 and ε_2 is assumed to be close to zero (or unknown), the error covariance matrix \mathbf{C} in (5) is a diagonal matrix and (5) leads to a common least squares problem:

$$\left\{ \sum_{i=1}^2 \frac{1}{\text{var}(\varepsilon_i)} [y_i - f_i(x)]^2 + \frac{1}{\text{var}(d_{0,ref})} [\hat{d}_{0,ref} - d_0]^2 \right\} \quad (7)$$

If *a priori* information on the temporal changes of SWE is available, this information can be also used to regulate the algorithm. In practice, this is reasonable when a time-series of brightness temperature observations are analysed. In that case (7) modifies to:

$$\left\{ \sum_{i=1}^2 \frac{[y_i - f_i(x)]^2}{\text{var}(\varepsilon_i)} + \frac{[\hat{d}_{0,ref} - d_0]^2}{\text{var}(d_{0,ref})} + \frac{[W_{t-1} - W_t]^2}{\text{var}(W_t)} \right\}, \quad (8)$$


where W_{t-1} denotes the level of SWE on the day prior to the day under investigation and the variance of day-to-day changes in SWE is denoted by $\text{var}(W_t)$.

Formulation (8) defines the inversion algorithm applied in this investigation. The algorithm considers the effect of possibly available *a priori* information. This is performed by weighing the satellite data (the first term of (8)) and reference information on snow grain size with their estimated statistical accuracy.

Assimilation technique

The data-assimilation technique applies a single channel difference, y_1 of (1). That is, the brightness temperature difference between vertically polarized SSMIS channels of 19.0 and 37.0 GHz is used. This channel difference is the most used index to derive SWE or SD (Chang et al. 1987). Again, the brightness temperature difference between the two channels is modelled by the HUT snow emission model. A maximum *a posteriori* probability of SWE or SD, when certain values of brightness temperatures are observed, is searched through the iterative inversion procedure analogously to (7). Ground-based (interpolated) SWE or SD value is employed as statistical *a priori* information. When meteorological synoptic SD observations are employed as a source of *a priori* information, the obtained SD estimates are converted to SWE estimates by multiplying them with snow density values that are regional and seasonal averages obtained from snow climatology (in case of testing the algorithm for Finland the climatology is obtained from snow course observation data).

SWE (or SD) estimates for all locations are interpolated from distributed synoptic observations and these values are applied as *a priori* estimates on SWE, when the scene brightness temperature model is fitted to space-borne observations by optimizing the value of SWE. In the fitting procedure, the *a priori* SWE-value is weighed with its modelled statistical uncertainty determined using spatial data analysis techniques (Kriging interpolation). As well, the radiometer data is weighed with the

	Algorithm Theoretical Baseline Document ATBD-65 (Product – SN-SWE-HH)	Doc.No: SAF/HSAF/ATBD-65 Rel. 1.2 Date: 11/11/2021 Page: 13/ 37
---	---	--

estimated accuracy of brightness temperature modelling. In that case, weighing factors are determined by analysing how well the brightness temperature model describes the radiometer observations at the locations of synoptic observations for the day under investigation (in that phase the consideration of snow grain size is included in the algorithm). The inclusion of (interpolated) SWE estimates as *a priori* data regulates the optimization procedure. Hence, the assimilation can be performed using a single channel difference y_1 of (9), i.e., using the channel difference that has the highest correlation with SWE.

We can write the assimilation algorithm as a three-stage optimization procedure (see Fig. 04 for the illustration).

The first phase of the algorithm is the estimation of effective snow grain size at the locations of reference stations, for which SD is observed. The grain size estimation is conducted by fitting the modeled brightness temperature difference into the brightness temperature difference observed by the instrument:

$$(y_1 - f_1(\rho, D, d_0))^2, \quad (9)$$

where D is the observed snow depth and ρ is snow density (note that $W=D\rho$). ρ is treated as a constant (using a temporal mean value from monthly snow climatology).

The procedure (9) is repeated for all reference stations for the day under investigation. The snow grain size for an arbitrary location (x, y) is then assumed to be equal to the mean of snow grain size estimated at its near-by-stations:

$$\langle \hat{d}_{0,\text{ref}} \rangle = \frac{1}{M} \sum_{j=1}^M \hat{d}_{0,\text{ref},j}, \quad (10)$$


where M is the number of reference stations in the neighbourhood of the location under investigation. Nine closest stations are used in case of testing for Finland and four closest for Eurasia. In Finland, the maximum distance between neighbouring stations is less than 100 km, but in the Eurasian case this distance exceeds 1000 km, which causes the low value, $M = 4$. For Northern America the situation is comparable to Eurasia since the station distance can exceed 1000 km (maximum distance might be as large as 3000 km).

According to (10), the standard deviation of the effective snow grain size is estimated by

$$\lambda_{d0,\text{ref}} = \sqrt{\frac{1}{M-1} \sum_{j=1}^M (\hat{d}_{0,\text{ref},j} - \langle \hat{d}_{0,\text{ref}} \rangle)^2}. \quad (11)$$

The second stage of the algorithm is the determination of SWE or SD estimate and its standard deviation for the location under investigation (x, y) from a set of distributed ground-based observations. Kriging interpolation (ordinary Kriging) is applied to synoptic SD observations, and SWE is estimated from the SD-values by multiplying them with snow density reference information. In contrast to block averaging of (10), the Kriging interpolation considers the spatial autocorrelation of snow depth (the required semivariogram is estimated from the discrete SD observations). The resulting estimates are:

- Interpolated SWE estimate \hat{W}_{ref} for the location under investigation (x, y) .

	<p>Algorithm Theoretical Baseline Document ATBD-65 (Product – SN-SWE-HH)</p>	<p>Doc.No: SAF/HSAF/ATBD-65 Rel. 1.2 Date: 11/11/2021 Page: 14/ 37</p>
---	--	--

- Standard deviation of the interpolated SWE estimate $\lambda_{W,ref}$, i.e. the statistical accuracy of the interpolated SWE estimate for the location $(x, y)_z$

The third phase of the algorithm is the estimation of SWE for the location (x, y) at the moment of time (day) t by weighing the two data sources by their estimated variances:

$$\left(\frac{(T_{B,19V,mod}(W_t) - T_{B,37V,mod}(W_t)) - (T_{B,19V,obs} - T_{B,37V,obs})}{var(\varepsilon_1, t)} \right)^2 + \left(\frac{W_t - \hat{W}_{ref,t}}{\lambda_{W,ref,t}} \right)^2 \quad \text{such as } W_t \geq 0 \text{ mm} \quad (12)$$

.Fig 03 shows the general flow chart of the assimilation method indicating how different contributions of (12) are estimated.

The third term in summation is an optional term that regulates the magnitude of day-to-day changes in SWE (λ_W is the standard deviation of day-to-day changes in snow water equivalent). In the first term of (12), the standard deviation of random error in modelled brightness temperature difference $\varepsilon_{1,t}$ is estimated from the estimated standard deviation of effective snow grain size (λ , see (11)) through the linearization of the relation between the brightness temperature and snow grain size:

$$\Delta T_b(W_t, d_0) \approx \Delta T_b(W_t, \langle \hat{d}_{0,ref,t} \rangle) + \frac{\partial \Delta T_b(W_t, \langle \hat{d}_{0,ref,t} \rangle)}{\partial d_0} (d_0 - \langle \hat{d}_{0,ref,t} \rangle)$$

$$\Rightarrow \text{var}(\varepsilon_{1,t}) = \text{var}(\Delta T_b(W_t, \langle \hat{d}_{0,ref,t} \rangle)) = \left(\frac{\partial \Delta T_b(W_t, \langle \hat{d}_{0,ref,t} \rangle)}{\partial d_0} \right)^2 \lambda_{d0,ref,t}^2 \quad (13)$$

where $\Delta T_B = y_1$.

Note that $\text{var}(\varepsilon_{1,t})$ in (13) is a function of SWE (denoted by W_t). When compared to (7) and (8), a major difference arises from the difference in determining the value of the term $\text{var}(\varepsilon_{1,t})$. When the assimilation algorithm fits the modelled brightness temperature difference into the observed value at the locations of reference station according to (9), the only fitting parameter to be optimized is the effective snow grain size d_0 . Hence, the total modelling error evident for every location between the reference stations is reduced to the spatial inaccuracy of effective d_0 . As an outcome, the variance of modelling error, $\text{var}(\varepsilon_{1,t})$ in (12), has to be determined as a function of snow grain size variance by (13).

[Note] SWE mapping has a problem over lakes, because MW instruments may see the liquid water which may lie between ice and snow. As for large lakes (e.g., Ladoga), the amount of snow is considerably less on their area than around them, so the synoptic weather data used as background in assimilation may overestimate the amount of snow. For small lakes with low fractional coverage in a pixel the impact is lower, but the possible accuracy implications need to be studied further.

3.2 Mountainous regions

[METU]

Snow emission model

The HUT snow emission model, which is described in section 3.1, is used in mountainous algorithm. Input and output schema of HUT model is given in Figure 5. Extinction coefficient κ_e used in the

original model is based on an experiment done by Hallikainen et al. (1987). They measured properties of 23 snow samples and used 18 of them for determining empirical relationship between extinction coefficient of snow against grain size(d_o) and frequency (f). The obtained empirical relationship is given in equation (14)

$$\kappa_e = 0.0018 f^{2.8} d_o^{2.0} \quad (14)$$

A modified relationship for modelling extinction coefficient based on Hallikainen's data is proposed and given in Equation (15)

$$\kappa_e = 0.08 f^{1.75} d_o^{1.8} \quad (15)$$

This modified equation gives R-square for 18GHz as 0.83 and for 35 GHz as 0.83 and the relationship is presented in Figure 6. This modified relationship was used for H13 mountain product. The same equation is used for H65 mountain product.

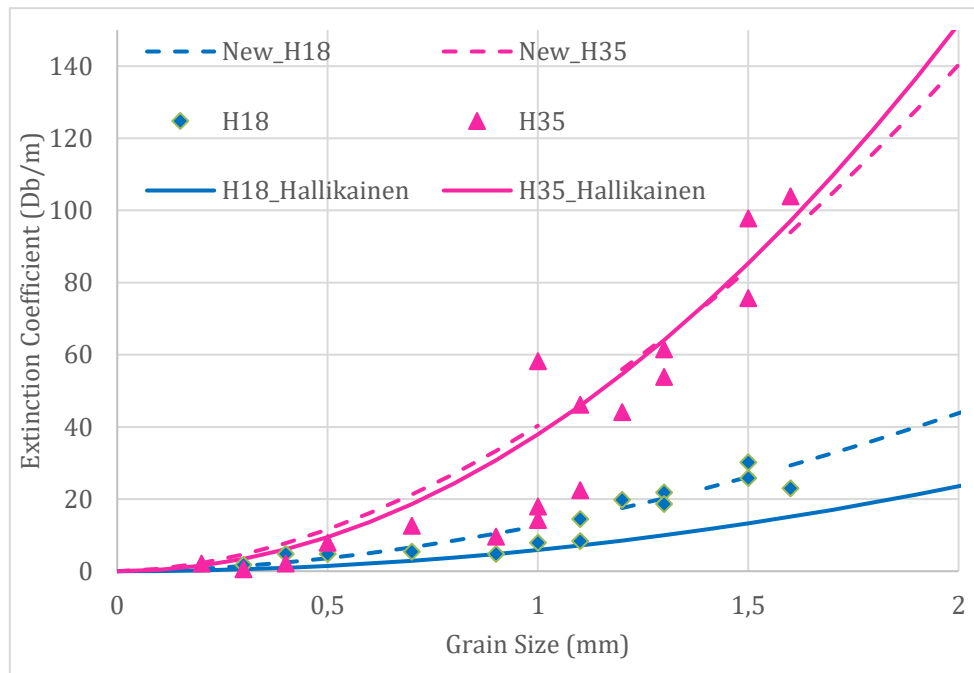


Figure 6 Measured extinction coefficients against grain size, fitted equation by Hallikainen et al. (1987) and the revised equation used in TSMS algorithm.

Performance of proposed extinction coefficient

The snow measurements considered in this study were conducted inside Karasu Basin which is located in the eastern part of Turkey. Snow observations are done by means of Automated Weather Observing Stations (AWOS) which measure snow depth every 10 minutes with ultrasonic snow depth sensor (Campbell SR50A model) operated by the Directorate of State Hydraulic Works (DSI). In this study Hacimahmut, Güzelyayla, Ovacik and Cat stations data were used. Elevations of these

stations are 1965 m, 2065 m, 2130 m and 2340 m respectively. Period of January 1st to March 15th of years 2003-2007 is analyzed. In this period snow is mostly in dry state. Snow density and temperature are measured twice in a month at these stations during snow courses. The snow density are measured in snow pits using snow tubes.

The input parameters of the HUT model include the snow pack characteristics (snow depth (SD), density (ρ), effective grain size (d_0), and temperature(T_s)), soil properties (temperature(T_g), effective soil surface roughness (RMS) variation(rm), moisture content (mv_g)) and near-surface air temperature. Table 3 summarizes typical values of fixed model parameters, as the HUT model is applied to the inversion of space- borne data. These values are obtained from the sensitivity analysis performed with AMSR-E data in 2012. For any AMSR-E pixel that includes any AWOS, it is assumed that station measured snow depth and density are homogenous inside that pixel. Therefore, only unknown parameter for that pixel is mean grain size of snowpack. From that analysis retrieval is found insensitive to snow temperature (-10°C - 0 °C) soil moisture content (0 - 0.2%), ground roughness (0 - 0.003 m), air temperature (-15°C - 5°C) and snow salinity (0 - 0.2 %) (Sorman and Beser, 2012).

Table 3 Prefixed HUT model parameters

Parameter	Value
Snow Temperature , T_s	-3°C
Snow moisture content, mv	0%
Effective soil surface roughness, rm	2 mm
Soil temperature, T_g	-1°C
Soil moisture content, mv_g	1%

Assimilation technique

The assimilation technique followed for mountainous part differs from the one followed for flat/forest part. Since no snow depth (SD) at Synoptic observation stations are used in mountainous assimilation part, a simple Monte Carlo simulation is followed. This assimilation technique applied in H13 for mountainous product is the same for H65. In order to calculate SWE in each domain pixel one should calculate snow density and snow depth for the particular pixel in interest. Calculation of these two parameters is done by inversion of HUT emission model. Inputs of the HUT model is depicted in Figure 5 and prefixed values are listed in Table 3. The only unknown parameters are snow depth, snow density and effective grain size of snow layer.

An empirical relationship between grain size, snow depth and brightness temperature difference of vertically polarized channels 19 GHZ and 37 GHz is used. The relationship is given in Equation (16) as

$$\frac{SD}{\Delta T_B} = ae^{b(d_0)} \Rightarrow SD = (ae^{b(d_0)})\Delta T_B \quad (16)$$

where d_0 is grain size; SD is snow depth; $\Delta T_B = T_{B,19} - T_{B,37}$

The a and b coefficients for each month during dry snow period was searched using calculated grain sizes by HUT model. Results for January, February and March is given in Table 4. All three months correlation coefficients are higher than 0.80.

Table 4 - Calculated a and b coefficients for January, February and March using equation (16)

Month	a	b	RMSE	R ²	%95 a	%95 b	Sample Number
January	21.94	-2.844	0.2344	0.8734	19.76, 24.12	-2.966, -2.721	351
February	19.87	-2.666	0.2095	0.912	18.43, 21.31	-2.759, -2.574	341
March	17.14	-2.378	0.3098	0.8289	14.72, 19.57	-2.561, -2.196	141

Mean densities by using Equation (17), which is obtained by rewriting Equation 16, are obtained for months January, February and March.

$$\frac{SD}{\Delta T_B} = ae^{bd_0} \Rightarrow \frac{\rho SD}{\Delta T_B} = \rho ae^{bd_0} \Rightarrow \frac{SWE}{\Delta T_B} = \rho ae^{bd_0}$$

$$\ln(\rho) = \ln\left(\frac{SWE}{\Delta T_B}\right) - \ln(a) - bd_0 \quad (17)$$

The calculated and the average of measured snow densities are given in Table 5. Since the comparison between the calculated and measured snow densities are close, Equation 17 is used in the HUT model.

Table 5 Calculated and measured snow densities at three AWOS

	JANUARY		FEBRUARY		MARCH	
	CALC	MEAS	CALC	MEAS	CALC	MEAS

GUZELYAYLA	0.25	0.25	0.27	0.27	0.30	0.30
OVACIK	0.22	0.21	0.25	0.24	0.28	0.28
CAT	0.28	0.30	0.28	0.30	0.30	0.32

Using the equation 18 to relate snow density to grain size, the parameters in the equation are calculated by using the measured snow densities. Calculated x and y coefficients and respective RMSE are presented in Table 6.

$$\rho = xd_0^5 + y \quad (18)$$

Table 6 Calculated x and y coefficients for equation (18)

Month	x	y	RMSE
JANUARY	-0.04727	0.2797	0.04056
FEBRUARY	-0.03738	0.2871	0.04278
MARCH	-0.01711	0.3015	0.05037

For every pixel, HUT model is run by assuming snow depth from 0.05 m to 1.00 m by 0.05 depth intervals. For every assumed snow depth, the grain size and snow density are calculated by using the empirical equations explained earlier (Equations 17 and 18). The simulation continues till the measured and modelled brightness temperature difference at 19 GHz and 37 GHz vertical channels is minimized. During this stage snow grain size is dynamically calculated using Equation (17) with selected empirical coefficients and density is calculated by inserting obtained grain size to Equation (18). As a result, the depth value which leads to smallest brightness temperature error is selected as that pixel's snow depth value. Density of that particular pixel is also calculated by Equation (18). SWE of the pixel is assigned as multiplication of calculated snow depth and density.

Snow density Look-up table

The continuous validation of H13 product over mountainous areas indicate the underestimation of the snow density in some areas (PVR documents, <https://hsaf.meteoam.it/Products/ProductsList?type=snow>). Mean monthly snow density values obtained from H13 snow product for mountainous areas are presented for 2010 and 2019 in Figure 7 and Figure 8, respectively.

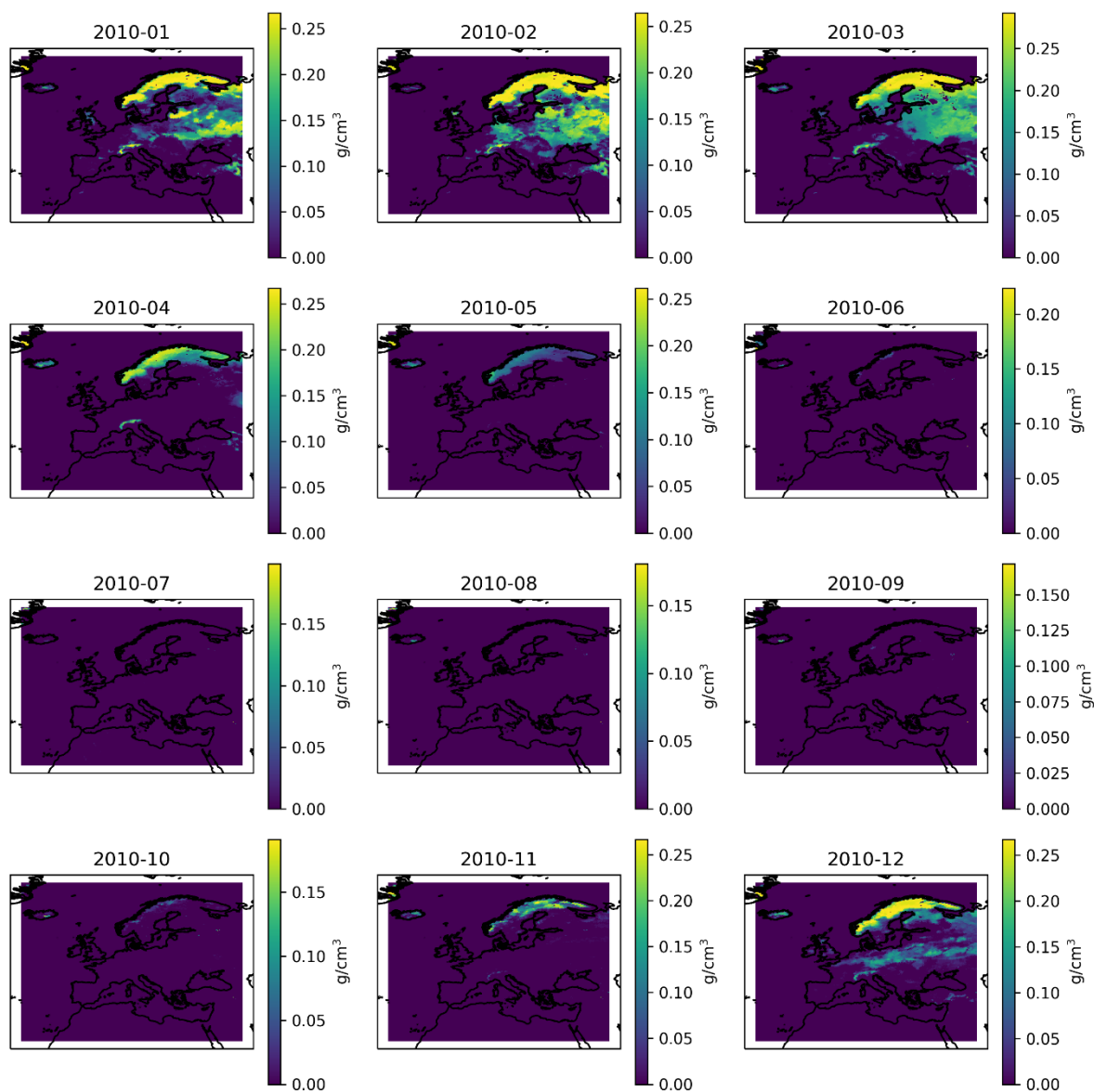


Figure 7 Spatial variation of Snow density retrieved from H13 product for 2010.

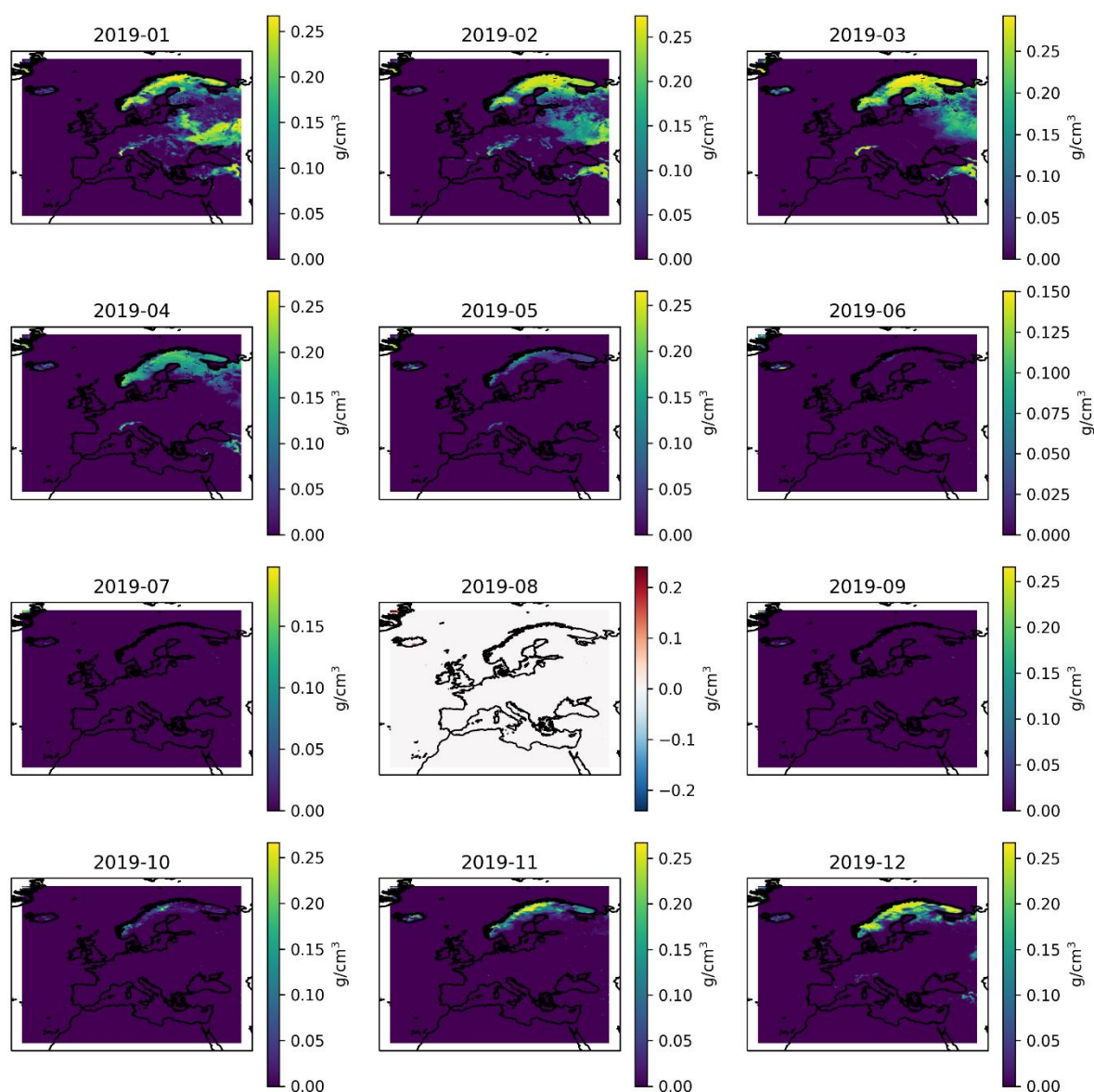


Figure 8 Spatial variation of Snow density retrieved from H13 product for 2019. (Due to a problem in the SSMI/S data snow density could not be retrieved for August)

The snow density variation in time for a particular location selected from Alps and Turkey is presented in Figure 9. The values present that snow density retrieved from H13 product for the mountainous areas are comparatively low for Alps and the figures show an unexpected variation in snow density among the years. Mauro et al. (2014) state that the most common density values measured for snowfalls in the Italian Alps are between 50 and 175 kgm⁻³ (83% of observations). Using measured air temperatures, during the 24 hours period for each station. With minimum air temperatures between +4° C and +1° C, the measured average fresh snow density was 188 kgm⁻³ (1% of the measurements), between 0° C and -4° C, such value increases between 160 and 114 kgm⁻³ (39 % of the measurements), between -5° C and -11° C its almost stationary (113-100 kgm⁻³, 49% of the measurements), between -12° C and -16° C its average is of 93 kgm⁻³ (9 % of the

measurements) and between -17°C and -21°C , it decreases to 73 kg m^{-3} (2 % of the measurements). According to Mauro et al. (2018), minimum snow density occurs in February (105 kg m^{-3}) and maximum density occurs in May (163 kg m^{-3}). According to Ertas and Sorman (2019), the long term average snow depth, snow density and snow water equivalent observed at the stations located between 1660-2400 m, for the period of 1964-2017 are 56 cm, 280 kg/m^3 and 160mm. The majority of the snow density values retrieved from H13 product from the Alps are lower than 60 kg m^{-3} and from Turkey lower than 250 kg/m^3 .

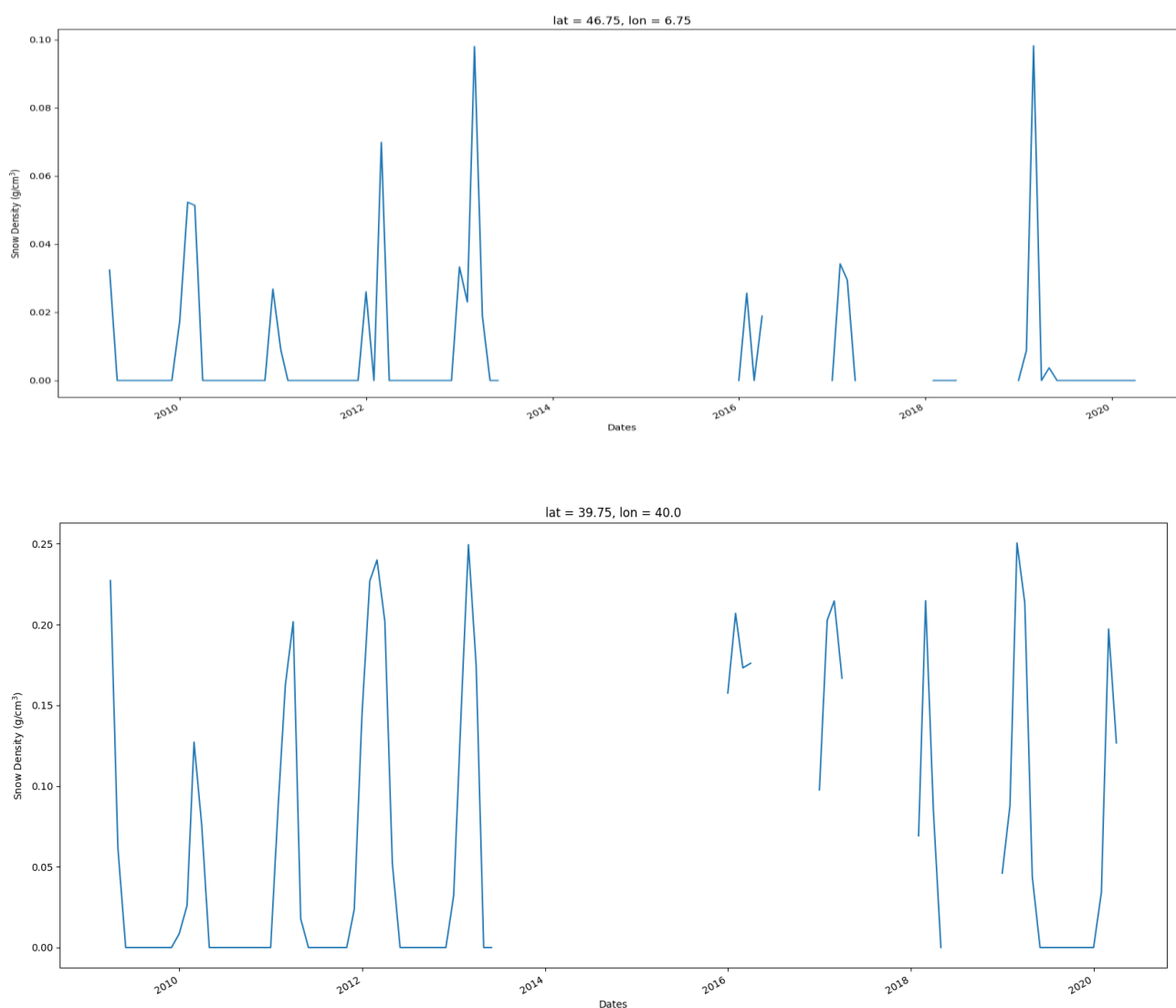


Figure 9 Temporal variation of Snow density retrieved from H13 product

ERA5-Land is a climate reanalysis product generated by the ECMWF with a long temporal coverage from 1950 to present, and it provides hourly data on various atmospheric, land-surface and sea-state parameters together with estimates of uncertainty (Hersbach et al., 2020). Snow density provided in ERA5-Land hourly data (Sabater, 2019) are downloaded from the associated web page

of Copernicus

(<https://cds.climate.copernicus.eu/cdsapp#!/dataset/10.24381/cds.e2161bac?tab=overview>).

Mean monthly snow density values obtained from ERA5-Land product are presented for 2010 and 2019 in Figure 10 and Figure 11, respectively.

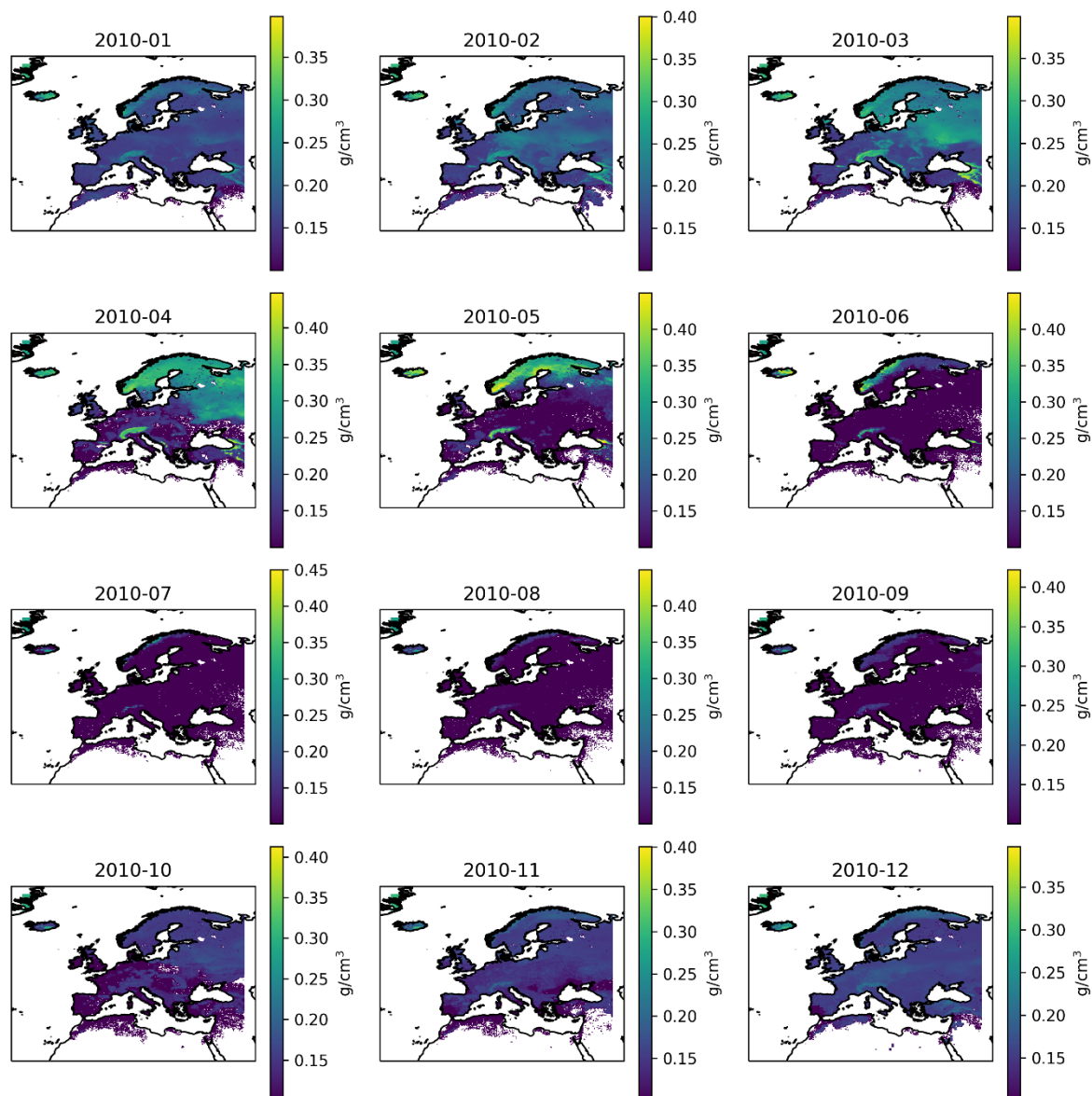


Figure 10 Spatial variation of Snow density retrieved from ERA5-Land product for 2010.

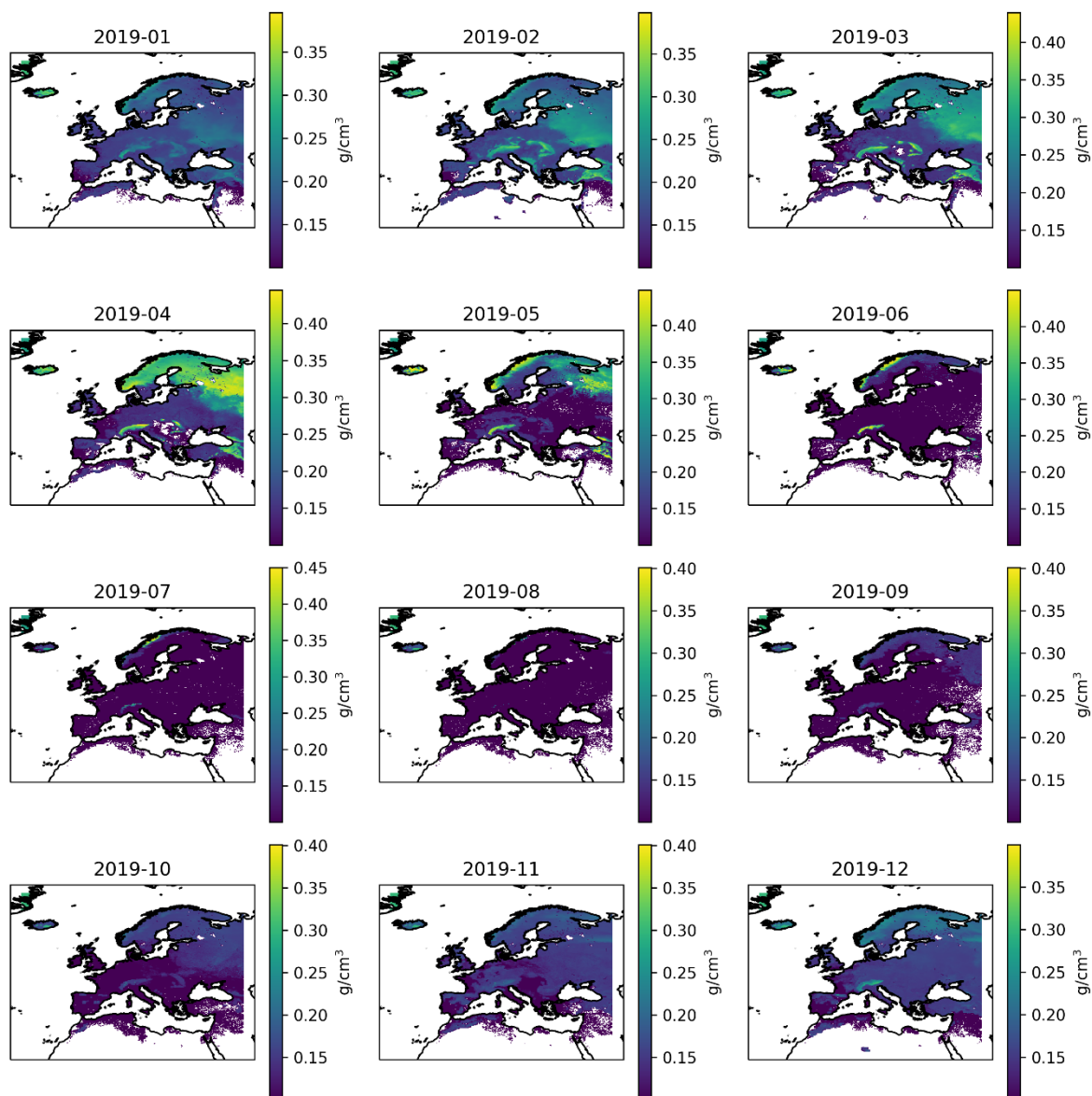


Figure 11 Spatial variation of Snow density retrieved from ERA5-Land product for 2019.

The snow density variation in time for a particular location selected in Alps and Turkey is presented in Figure 12. The values present that snow density retrieved from ERA5-Land product for the mountainous areas are comparatively low for Alps and the figures show an unexpected variation in snow density among the years.

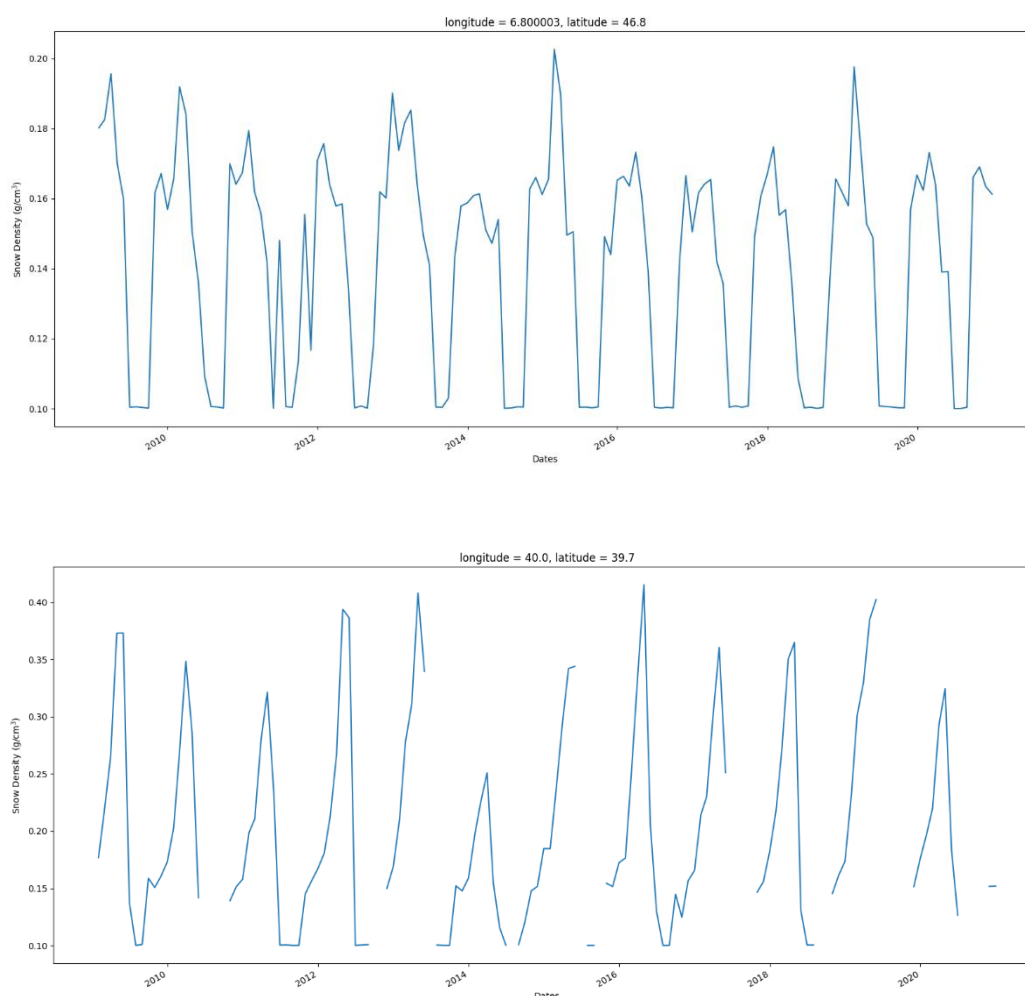



Figure 12 Temporal variation of Snow density retrieved from ERA5-Land product

Since the ERA5-Land snow densities show more realistic spatial and temporal variations, a look up table for snow density for the whole domain is developed and it is included in SWE assimilation methodology. If an unrealistic snow density ($\rho < 0.1$) is obtained during SWE assimilation, it is replaced with the snow density from the look up table. As a result, the depth value which leads to smallest brightness temperature error is selected as that pixel's depth value. Density of that particular pixel is obtained from the lookup table. SWE of the pixel is assigned as multiplication of calculated snow depth and density.

Since SD from Synoptic ground observations are not used during the assimilation stage for mountainous part, there is no uncertainty estimate calculation for the mountainous part. The retrieval error is calculated during the validation activity for each snow year. The validation methodology is followed for the dry snow condition. In-situ measurements can be compared individually with the corresponding 25x25 km² SSMI/S footprint. For each measurement location the elevation of the weather station or ground measurement should be compared against the SSMI/S pixel median elevation where the measurement falls inside it. The product SWE values are

	<p>Algorithm Theoretical Baseline Document ATBD-65 (Product – SN-SWE-HH)</p>	<p>Doc.No: SAF/HSAF/ATBD-65 Rel. 1.2 Date: 11/11/2021 Page: 25/ 37</p>
---	--	--

compared with the ground observations and the validation results are presented in RMSE. Detailed information can be found in Product Validation Report (PVR) of H13.


3.3. Key differences to H13 SWE product and between FMI and TSMS algorithms

The key differences to H13 SWE product are:

- 1) The H13 SWE product covers the H SAF European domain which is 25-75°N lat, 25°W-45°E long with nominal 0.25 degrees resolution. The SN-SWE-HH (H65) covers Northern Hemisphere in the EASE-Grid 2.0 (The Equal-Area Scalable Earth) (Brozik et al. 2012, 2014). The nominal resolution of H65 is 25 km which is comparable to the resolution of H13.
- 2) The H13 uses the original HUT model (Pulliainen et al. 1999) whereas SN-SWE-HH (H65) now has updated HUT model (Lemmetyinen et al. 2010). The main differences are the possibility to use multi-layer emission model and consider the effect of lake ice. Even though the SN-SWE-HH is implemented using single layer model the future enhancement of the product is thus possible.
- 3) Variable snow depth variance for different land usage categories (forest, tundra). The variance for tundra is 400 cm² and for forest 150 cm². The rationale behind this is that over tundra the snow is usually much more wind driven and the depth varies more. This improvement does have a minor improvement over the SWE retrieval.
- 4) The H13 product does provide flags for the status of the SWE retrieval. However, the SWE-SN-HH (H65) will provide an uncertainty estimate describing the total product (SWE) error for flat areas (FMI). It consists of a statistical random error component and systematic error component. The statistical component is estimated using an error propagation analysis (Salminen et al.) and the systematic error component is determined using snow transect reference data. In particular, the statistical component is a theoretical error that considers the spatially and temporally varying characteristics of the weather station snow depth (SD) observations and the spaceborne derived (microwave radiometer) measurements. The systematic component on the other hand contains all other error factors such as inaccuracies in the forward modelling etc. The systematic error is the residual of the total error (derived from transect data) and the statistical error.
- 5) For mountain part, the domain is enlarged to Northern Hemisphere in the EASE-Grid 2.0 (The Equal-Area Scalable Earth) (Brozik et al. 2012, 2014). The nominal resolution of H65 is 25 km which is comparable to the resolution of H13.
- 6) A look-up table of snow density is included for the erroneous densities obtained during assimilation.

The key differences between FMI and TSMS algorithms:

In both algorithms HUT snow emission model is used for the assimilation of 19V, 37V brightness temperature of SSMIS data. Both algorithms use single layer emission model. However, in FMI algorithm snow depth observed at stations are used in the HUT model inversion to obtain an estimate of snow grain size (fitting parameter) for the station locations. In TSMS algorithm ground observations are not used. Because any interpolation of ground observation of SD would bring extra

	Algorithm Theoretical Baseline Document ATBD-65 (Product – SN-SWE-HH)	Doc.No: SAF/HSAF/ATBD-65 Rel. 1.2 Date: 11/11/2021 Page: 26/ 37
---	---	--

error in complex topography. Therefore, SD values are obtained through Monte Carlo simulations during the assimilation.

In FMI algorithm the snow grain size estimate (and error) are interpolated for the target area. In TSMS algorithm retrieval error is not calculated since no ground observations are used in the assimilation. The error is calculated during the validation activity for each snow year. The validation methodology is followed for the dry snow condition. In-situ measurements can be compared individually with the corresponding 25x25 km² SSMI/S footprint. For each measurement location the elevation of the weather station or ground measurement should be compared against the SSMI/S pixel median elevation where the measurement falls inside it.

3.4. Assumptions and Limitations

Both algorithms have certain limitations.

- FMI algorithm does not work over land or sea ice
- FMI algorithm works best when SWE<150mm and then underestimates the SWE.
- FMI algorithm is not applied to mountains. The coarse spatial resolution and the penetration characteristics of the SSMI/S instrument for shallow and deep snow lead under and over estimation in the SWE retrieval.
- Mountainous Algorithm underestimates SWE when SWE is larger than 150 mm. This is a typical behaviour of the algorithm since with large values of SWE, the signal of the radiometer is saturated.

3.5. Merging

Although the products for flat/forested areas and for mountainous areas generated by FMI and TSMS cover the full Northern Hemisphere, their quality differs in different areas, the product from FMI being tuned for flat/forested areas, that one from TSMS being tuned for mountainous areas. However, a single product is distributed to the users, obtained by merging the two products in such a way that in flat/forested areas the FMI product is captured, and in mountainous areas the TSMS product is captured. The distinction is determined by the “mountain mask” shown in Figure 1, that was defined by METU.

A mask based on digital elevation model (DEM) was used to separate the mountainous pixels from flat/forested areas. The merging algorithm finds the location of the non-mountainous pixels using this mask (Ertürk, 2009).

The flow chart for merging procedure is given in Figure 13. First, the availability of the FMI and TSMS part are checked. If FMI part is missing it is replaced by plain landmask. If the TSMS part is missing it is replaced by NODATA values using mountain mask. Second, the FMI part is used as basis for the merging. According to the mountain mask, the mountain pixels are then replaced with the TSMS data (or NODATA if the part is missing).

The final merged product consists of the merged SWE product but the FMI and TSMS are parts are also provided as channels of the resulting netCDF file.

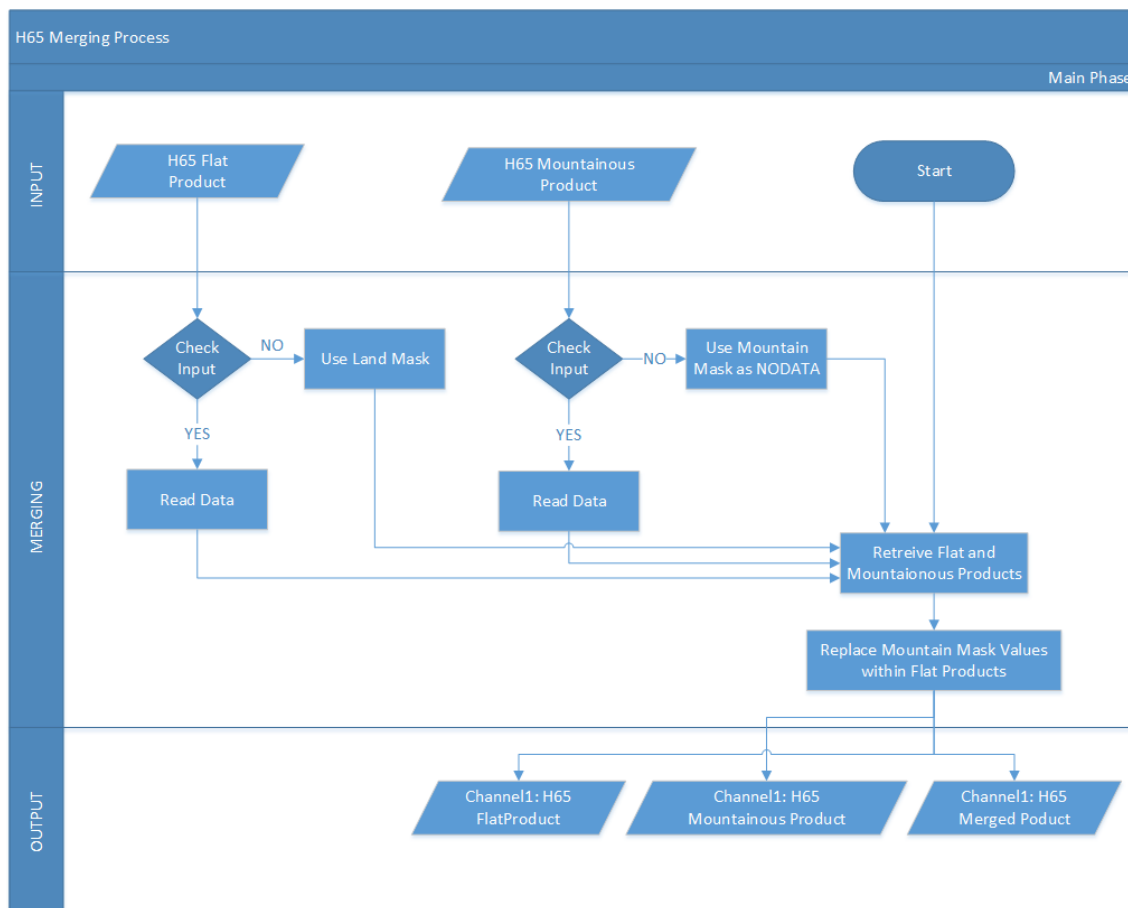


Figure 13 The flowchart of the merging process of H65

4 Validation *<if applicable>*


5 Examples *<if available>*

6 Connections to other projects and future evolution of SWE products

FMI provides Snow Water Equivalent (SWE) estimates as Climate Data Record (CDR) or Near Real Time (NRT) services. In general, the idea is to have the bleeding edge scientific product development in the CDR context and then later to introduce it to operational NRT services.

The FMI SWE algorithm has different internal baseline versions with improvements between the major versions. The versions, their differences and relevance to projects are listed in following table.

FMI SWE Version	Product context	Version properties	Relevant Project
1.3	NRT (Takala et al. 2011) T [1]	<ul style="list-style-type: none"> -SWE as the data fusion of synoptic observations and space borne derived estimates (~25 km) -Error field is only the kriging interpolation error -No mountains -Optical snow mask from VIIRS derived Snow Extent (SE) data applied -SSMIS as the radiometer data source -For user convenience SWE is interpolated to ~5 km resolution -covers Northern Hemisphere 	COPERNICUS
2.0	NRT	<ul style="list-style-type: none"> - SWE estimate with improved emission model - Possibility to consider effect of frozen lakes - possibility to consider multilayer snowpack - Variable snow variance for different land use categories - SWE error contains systematic error component -> error field is the real SWE estimate error - no optical mask (radiometer) - mountains included as the Turkish TSMS contribution - Algorithm is tested to work with other radiometer data than SSMIS (Chinese FY) - Once relevant EPS-SG Metop is launched the product will be updated to use MWI (Microwave Radiometer) making it distinctively EUMETSAT product H665 - Covers Northern Hemisphere 	EUMETSAT H SAF H65
2.1	NRT (Takala et al. 2017)	<ul style="list-style-type: none"> -True improved resolution (~5 km) using super resolution algorithm - Covers Northern Hemisphere -improved auxiliary files -IMS used as snow mask -Possibility to use MWI data as source -will include mountains 	Proposed (CDOP 4) EUMETSAT H SAF super resolution product H66 & H666

	Algorithm Theoretical Baseline Document ATBD-65 (Product – SN-SWE-HH)	Doc.No: SAF/HSAF/ATBD-65 Rel. 1.2 Date: 11/11/2021 Page: 29/ 37
---	---	--

FMI SWE Version	Product context	Version properties	Relevant Project
3.0	CDR (Pulliainen et al. 2020)	- no NRT service, only annual updates of the climate data record -In comparison to NRT products the CDR uses harmonized synoptic data -no mountains -Improved model of effect of vegetation -Will be introduced to NRT domain (that is H SAF context) in the future	ESA Snow CCI

Table 8 - FMI SWE algorithm baseline versions and their properties and relevance to different projects

EUMETSAT H SAF vs COPERNICUS

The COPERNICUS SWE product is in principle the established GlobSnow v1.3 SWE product which combines information from optical satellite based EO data, the product combines the snow line information from optical instrument, improving the snow delineation in large number of cases and is therefore packaged for a 5km output grid, serving specific heritage end user segments. The product does not contain information for the mountainous regions. Further, it's a combination of GS SWE and Snow Extent (SE) based on VIIRS optical sensor. Second, the intrinsic resolution of the SWE base field remains ~25 km, even as the regridding with the optical data allows a ~5 km grid for end user convenience.

All the development and research work that has been conducted since GlobSnow project are introduced to EUMETSAT H SAF project. The most important improvement for end user is the real estimate on SWE accuracy even though there are also major improvements in many parts of the algorithm. The COPERNICUS SWE doesn't contain mountainous areas. One of the advantages of the H65 product is thus the TSMS SWE part from Turkey. The proposed H SAF super resolution SWE product in CDOP 4 will give a true resolution improvement from ~25 km to ~5 km (Takala et al. 2017). The H65 and H66 products, as well as their evolution for EPS-SG MWI, will cover the Northern Hemisphere.

The FMI SWE algorithm version 2.x has been exclusively tested with different radiometer data input. In particular, the Chinese Fengyun space borne radiometer data works as well as SSMIS with the algorithm. Once relevant Metop satellite(s) in the EUMETSAT EPS-SG program are launched the H SAF SWE products are foreseen to be upgraded to use Metop Microwave Imager (MWI) data as input. This will further consolidate the uniqueness of the SWE products as exclusively EUMETSAT products. From the product continuation point of view, it is very important that new radiometer data sources are tested and available.

EUMETSAT H SAF vs ESA Snow CCI

From the table 8. one can deduce that ESA Snow CCI is a development and research project aiming at the generation of best available CDR for scientific purposes. The FMI SWE algorithm is the best algorithm in the world now (Pulliainen et al. 2020). However, the Snow CCI project is not producing a near-real time service, the climate data record is updated in an annual basis. It makes sense that EUMETSAT H SAF Snow product portfolio contains a near-real time SWE product. The FMI strategy concerning NRT products has all the time been to do main development and scientific research with CDR products and then later introduce them to operational NRT services. This applies exactly to the ESA Snow CCI project in relation to EUMETSAT H SAF. The Snow CCI development can and should be introduced to H SAF Snow portfolio in the future.

Evolution of H SAF SWE products in CDOP3 and CDOP4 The figure 14 presents the timeline of SWE product evolution in CDOP3 and CDOP4 phase. The current operational product will first be replaced with H65 offering the improvements over H13 described earlier. Once the Metop SG MWI instrument data becomes available the operational implementation of H65 will take advantage of it. Then the H65 will be replaced by H665.

In addition, the development of 5 km super resolution version of SWE for H SAF region will start. It will too be replaced with the MWI version (H666) in the future.

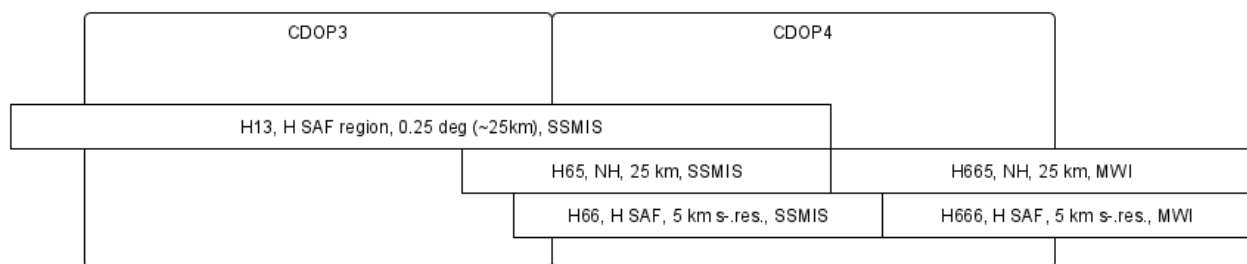



Figure 14. The timeline of SWE products in H SAF snow product portfolio

7 References

- Brodzik, M. J., B. Billingsley, T. Haran, B. Raup, M. H. Savoie. 2012. EASE-Grid 2.0: Incremental but Significant Improvements for Earth-Gridded Data Sets. *ISPRS International Journal of Geo-Information*, 1(1):32-45, doi:10.3390/ijgi1010032. <http://www.mdpi.com/2220-9964/1/1/32>.
- Brodzik, M. J., B. Billingsley, T. Haran, B. Raup, M. H. Savoie. 2014. Correction: Brodzik, M. J. et al. EASE-Grid 2.0: Incremental but Significant Improvements for Earth-Gridded Data Sets. *ISPRS International Journal of Geo-Information* 2012, 1, 32-45. *ISPRS International Journal of Geo-Information*, 3(3):1154-1156, doi:10.3390/ijgi3031154. <http://www.mdpi.com/2220-9964/3/3/1154>
- Chang A.T.C., J.L. Foster and D.K. Hall, 1987: "Nimbus-7 SMMR-derived global snow cover parameters". *Ann. Glaciol.*, 9, 39-44.

	<p>Algorithm Theoretical Baseline Document ATBD-65 (Product – SN-SWE-HH)</p>	<p>Doc.No: SAF/HSAF/ATBD-65 Rel. 1.2 Date: 11/11/2021 Page: 31/ 37</p>
---	--	--

Ertas, M.C. and A.A. Sorman, 2019: “Türkiye’nin Dağlık Doğu Bölgesi için Kar derinliğinden karsu eşdeğerinin belirlenmesi”. X. Hidroloji Kongresi. 927-936.

Ertürk A.G., 2009: “HSAF Visiting Scientist Activity at FMI. Final Report”. Hydro-SAF Visiting Scientist Report VS3_11.

Hallikainen M.T., F.T. Ulaby and T.E.V. Deventer, 1987: “Extinction behaviour of dry snow in the 18-to-90 GHz range”. *IEEE Transactions on Geoscience and Remote Sensing*, pp. 737-745.

Hersbach, H., Bell, B., Berrisford, P., Hirahara, S., Horányi, A., Muñoz-Sabater, J., Nicolas, J., Peubey, C., Radu, R., Schepers, D., Simmons, A., Soci, C., Abdalla, S., Abellan, X., Balsamo, G., Bechtold, P., Biavati, G., Bidlot, J., Bonavita, M., De Chiara, G., Dahlgren, P., Dee, D., Diamantakis, M., Dragani, R., Flemming, J., Forbes, R., Fuentes, M., Geer, A., Haimberger, L., Healy, S., Hogan, R.J., Hólm, E., Janisková, M., Keeley, S., Laloyaux, P., Lopez, P., Lupu, C., Radnoti, G., de Rosnay, P., Rozum, I., Vamborg, F., Villaume, S., and Thépaut, J.-N. (2020). The ERA5 global reanalysis. *Quarterly Journal of the Royal Meteorological Society*, 146, 1999-2049.

Kärnä J-P., J. Pulliainen, J. Lemmetyinen, M. Hallikainen, P. Lahtinen, and M. Takala, 2007: “Operational Snow Map Production for whole Eurasia using Microwave Radiometer and Ground-based Observations”. In *IEEE 2007 International Geoscience and Remote Sensing Symposium (IGARSS'07)*, Barcelona, Spain, July 24 - July 28, 2007.

Kruopis N., J. Praks, A.N. Arslan, H. Alasalmi, J. Koskinen and M. Hallikainen, 1999: “Passive microwave measurements of snow-covered forest areas in EMAC’95”. *IEEE Trans. Geosci. Remote Sensing* 37:2699-2705.

Lemmetyinen, J., Pulliainen, J., Rees, A., Kontu, A., Qiu, Y., Derksen, C., 2010: Multiple-layer adaptation of HUT snow emission model: Comparison with experimental data *IEEE Transactions on Geoscience and Remote Sensing* 48 (7), 2781-2794, 2010.

Mauro V., Chiambretti, I. and Dellavedova, P., 2014 “Fresh snow density on the Italian Alps” EGU General Assembly, held 27 April - 2 May, 2014 in Vienna, Austria, id.9715


Mauro V., Guyennon, N, Salerno, F., Petrangeli, A.B., Salvatori, R., Cianfarra, P. and Romano E., 2018. “Predicting new snow density in the Italian Alps : A variability analysis based on 10 years of measurements”. *Hydrological Processes*. <https://doi.org/10.1002/hyp.13249>

Pulliainen J. and M. Hallikainen, 2001: “Retrieval of regional snow water equivalent from space-borne passive microwave observations”. *Remote Sensing of Environment*, 75, 76–85.

Pulliainen J., 2006: “Mapping of snow water equivalent and snow depth in boreal and sub-arctic zones by assimilating space-borne microwave radiometer data and ground-based observations”. *Remote Sensing of Environment*, 101, 257-269.

Pulliainen J., J. Grandell and M. Hallikainen, 1999: “HUT snow emission model and its applicability to snow water equivalent retrieval”. *IEEE Trans. Geosci. Remote Sensing*, 37, 1378–1390.

Pulliainen J., J. Vepsäläinen, S. Kaitala, M. Hallikainen, K. Kallio, V. Fleming and P. Maunula, 2004: “Regional water quality mapping through the assimilation of spaceborne remote sensing data to ship-based transect observations”. *J. Geophys. Res.*, 109:C12009, doi:10.1029/2003JC002167.

	<p>Algorithm Theoretical Baseline Document ATBD-65 (Product – SN-SWE-HH)</p>	<p>Doc.No: SAF/HSAF/ATBD-65 Rel. 1.2 Date: 11/11/2021 Page: 32/ 37</p>
---	--	--

Pulliainen J., J.-P. Kärnä and M. Hallikainen, 1993: “Development of geophysical retrieval algorithms for the MIMR”. *IEEE Trans. Geosci. Remote Sensing*, 31:268-277.

Pulliainen, J., Luoju, K., Derksen, C., Mudryk, L., Lemmetyinen, J., Salminen, M., Ikonen, K., Takala, M., Cohen, J., Smolander, T. and Norberg, J. (2020). Patterns and trends of Northern Hemisphere snow mass from 1980 to 2018. *Nature* **581**, 294–298. doi:10.1038/s41586-020-2258-0.


Roy V., K. Goïta, A. Royer, A. Walker and B. Goodison, 2004: “Snow water equivalent retrieval in a Canadian boreal environment from microwave measurements using the HUT snow emission model. *IEEE Transactions on Geoscience and Remote Sensing*, 42, 1850-1859.

Sabater, M. (2019). ERA5-Land hourly data from 1981 to present. *Copernicus Climate Change Service (C3S) Climate Data Store (CDS)*, 10.24381/cds.e2161bac.

Salminen, M. *et al.* Determination of uncertainty characteristics for the satellite data-based estimation of fractional snow cover. *Remote Sensing of Environment* **212**, 103–113 (2018).

Takala M., Luoju K., Pulliainen J., Derksen C., Lemmetyinen J., Kärnä J.-P., Koskinen J., Bojkov B. (2011). Estimating northern hemisphere snow water equivalent for climate research through assimilation of space-borne radiometer data and ground-based measurements, *Remote Sensing of Environment*, Vol. 115, Issue 12, 15 December 2011, Pp. 3517-3529, doi:10.1016/j.rse.2011.08.014.

Takala M., Ikonen J., Luoju K., Lemmetyinen J., Metsämäki S., Cohen J., Arslan A. N. and Pulliainen J. 2017. New Snow Water Equivalent Processing System With Improved Resolution Over Europe and its Applications in Hydrology. *IEEE Journal of Selected Topics in Applied Earth Observations and Remote Sensing*, vol. 10, no. 2, pp. 428-436, doi: 10.1109/JSTARS.2016.2586179

	Algorithm Theoretical Baseline Document ATBD-65 (Product – SN-SWE-HH)	Doc.No: SAF/HSAF/ATBD-65 Rel. 1.2 Date: 11/11/2021 Page: 33/ 37
---	---	--

Annex1: Introduction to H-SAF

The EUMETSAT Satellite Application Facilities

H-SAF is part of the distributed application ground segment of the “*European Organization for the Exploitation of Meteorological Satellites (EUMETSAT)*”. The application ground segment consists of a “*Central Application Facilities*” located at EUMETSAT Headquarters, and a network of eight “*Satellite Application Facilities (SAFs)*”, located and managed by EUMETSAT Member States and dedicated to development and operational activities to provide satellite-derived data to support specific user communities (see Figure 7):

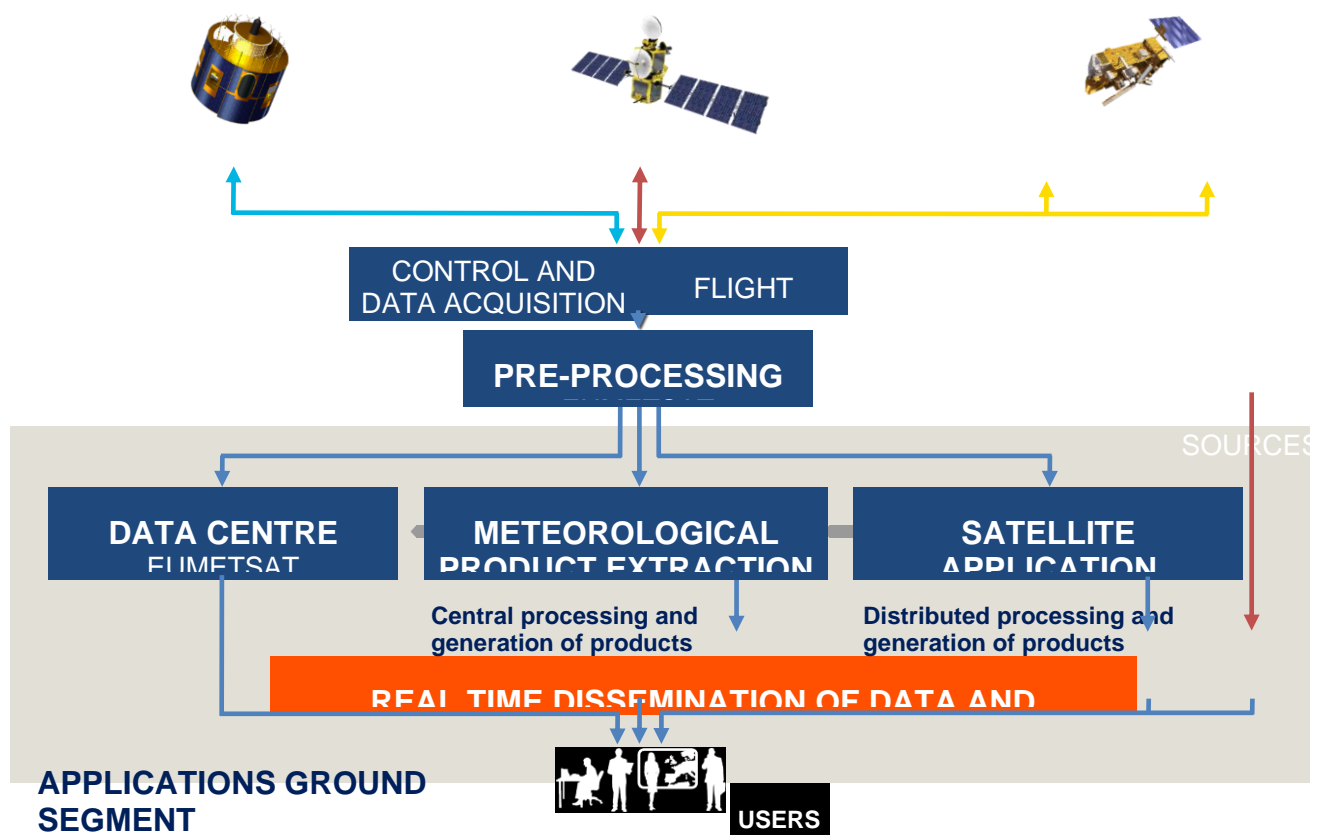


Figure 7: Conceptual scheme of the EUMETSAT Application Ground Segment

Figure 8 depicts the composition of the EUMETSAT SAF network, with the indication of each SAF's specific theme and Leading Entity.


	<p>Algorithm Theoretical Baseline Document ATBD-65 (Product – SN-SWE-HH)</p>	<p>Doc.No: SAF/HSAF/ATBD-65 Rel. 1.2 Date: 11/11/2021 Page: 34/ 37</p>
---	--	--




Figure 8: Current composition of the EUMETSAT SAF Network

Purpose of the H-SAF

The main objectives of H-SAF are:

- a. to provide new satellite-derived products** from existing and future satellites with sufficient time and space resolution to satisfy the needs of operational hydrology, by generating, centralizing, archiving and disseminating the identified products:
 - precipitation (liquid, solid, rate, accumulated);
 - soil moisture (at large-scale, at local-scale, at surface, in the roots region);
 - snow parameters (detection, cover, melting conditions, water equivalent);
- b. to perform independent validation of the usefulness of the products** for fighting against floods, landslides, avalanches, and evaluating water resources; the activity includes:
 - downscaling/upscaling modelling from observed/predicted fields to basin level;
 - fusion of satellite-derived measurements with data from radar and raingauge networks;
 - assimilation of satellite-derived products in hydrological models;
 - assessment of the impact of the new satellite-derived products on hydrological applications.

	Algorithm Theoretical Baseline Document ATBD-65 (Product – SN-SWE-HH)	Doc.No: SAF/HSAF/ATBD-65 Rel. 1.2 Date: 11/11/2021 Page: 35/ 37
---	---	--

Products / Deliveries of the H-SAF

For the full list of the Operational products delivered by H-SAF, and for details on their characteristics, please see H-SAF website hsaf.meteoam.it.

All products are available via EUMETSAT data delivery service (EUMETCast, <http://www.eumetsat.int/website/home/Data/DataDelivery/EUMETCast/index.html>), or via ftp download; they are also published in the H-SAF website hsaf.meteoam.it.

All intellectual property rights of the H-SAF products belong to EUMETSAT. The use of these products is granted to every interested user, free of charge. If you wish to use these products, EUMETSAT's copyright credit must be shown by displaying the words "copyright (year) EUMETSAT" on each of the products used.

System Overview

H-SAF is led by the Italian Air Force Meteorological Service (ITAF MET) and carried on by a consortium of 21 members from 11 countries (see website: hsaf.meteoam.it for details)

Following major areas can be distinguished within the H-SAF system context:

- Product generation area
- Central Services area (for data archiving, dissemination, catalogue and any other centralized services)
- Validation services area which includes Quality Monitoring/Assessment and Hydrological Impact Validation.

Products generation area is composed of 5 processing centres physically deployed in 5 different countries; these are:

- for precipitation products: ITAF COMET (Italy)
- for soil moisture products: ZAMG (Austria), ECMWF (UK)
- for snow products: TSMS (Turkey), FMI (Finland)

Central area provides systems for archiving and dissemination; located at ITAF COMET (Italy), it is interfaced with the production area through a front-end, in charge of product collecting.

A central archive is aimed to the maintenance of the H-SAF products; it is also located at ITAF COMET.

Validation services provided by H-SAF consists of:

- Hydrovalidation of the products using models (hydrological impact assessment);
- Product validation (Quality Assessment and Monitoring).

Both services are based on country-specific activities such as impact studies (for hydrological study) or product validation and value assessment.

Hydrovalidation service is coordinated by IMWM (Poland), whilst Quality Assessment and Monitoring service is coordinated by DPC (Italy): The Services' activities are performed by experts from the national meteorological and hydrological Institutes of Austria, Belgium, Bulgaria, Finland, France, Germany, Hungary, Italy, Poland, Slovakia, Turkey, and from ECMWF.

Annex 2: Acronyms

ATBD	Algorithms Theoretical Baseline Document
AU	Anadolu University (in Turkey)
BfG	Bundesanstalt für Gewässerkunde (in Germany)
CAF	Central Application Facility (of EUMETSAT)
CESBIO	Centre d'Etudes Spatiales de la Biosphère (of CNRS, in France)
CMSAF	SAF on Climate Monitoring
CNMCA	Centro Nazionale di Meteorologia e Climatologia Aeronautica (in Italy)
CNR	Consiglio Nazionale delle Ricerche (of Italy)
CNRS	Centre Nationale de la Recherche Scientifique (of France)
DEM	Digital Elevation Model
DMSP	Defence Meteorological Satellite Program
DPC	Dipartimento Protezione Civile (of Italy)
DWD	Deutscher Wetterdienst
ECMWF	European Centre for Medium-range Weather Forecasts
EOS	Earth Observing System (Terra, Aqua, Aura)
EUM	Short for EUMETSAT
EUMETCast	EUMETSAT's Broadcast System for Environmental Data
EUMETSAT	European Organisation for the Exploitation of Meteorological Satellites
FMI	Finnish Meteorological Institute
FTP	File Transfer Protocol
GEO	Geostationary Earth Orbit
GRAS-SAF	SAF on GRAS Meteorology
GTOPO	Global digital elevation model (U.S. Geological Survey)
H SAF	SAF on Support to Operational Hydrology and Water Management
HUT	Helsinki University of Technology (same as TKK)
IFOV	Instantaneous Field Of View
IMWM	Institute of Meteorology and Water Management (in Poland)
IPF	Institut für Photogrammetrie und Fernerkundung (of TU-Wien, in Austria)
IR	Infra Red
IRM	Institut Royal Météorologique (of Belgium) (alternative of RMI)
ISAC	Istituto di Scienze dell'Atmosfera e del Clima (of CNR, Italy)
ITU	İstanbul Technical University (in Turkey)
LATMOS	Laboratoire Atmosphères, Milieux, Observations Spatiales (of CNRS, in France)
LEO	Low Earth Orbit
LSA SAF	SAF on Land Surface Analysis
Météo France	National Meteorological Service of France
METU	Middle East Technical University (in Turkey)
MW	MicroWave
NASA	National Aeronautical and Space Administration (in USA)
NMA	National Meteorological Administration (of Romania)
NOAA	National Oceanic and Atmospheric Administration (Agency and satellite)
NWC	Nowcasting
NWC SAF	SAF in support to Nowcasting & Very Short Range Forecasting
NWP	Numerical Weather Prediction
NWP SAF	SAF on Numerical Weather Prediction

AC SAF	SAF on Ozone and Atmospheric Chemistry Monitoring
OMSZ	Hungarian Meteorological Service
OSI-SAF	SAF on Ocean and Sea Ice
PUM	Product User Manual
PVR	Product Validation Report
RMI	Royal Meteorological Institute (of Belgium) (alternative of IRM)
RMSE	Root Mean Square Error
SAF	Satellite Application Facility
SCA	Snow Covered Area
SD	Snow Depth
SHMÚ	Slovak Hydro-Meteorological Institute
SSM/I	Special Sensor Microwave / Imager (on DMSP up to F-15)
SSMIS	Special Sensor Microwave Imager/Sounder (on DMSP starting with S-16)
STD	Standard Deviation
SVRR	System Validation Results Review
SWE	Snow Water Equivalent
TSMS	Turkish State Meteorological Service
TU-Wien	Technische Universität Wien (in Austria)
UniFe	University of Ferrara (in Italy)
VIS	Visible
ZAMG	Zentralanstalt für Meteorologie und Geodynamik (of Austria)